periodontal ligament were derived from Hertwig's epithelial root sheath and dental follicles, respectively. However, recent studies have proposed that Hertwig's epithelial root sheath cells may not transform into cementoblasts, or multilineage differentiation of dental follicle cells might be due to *Runx2* overexpression enhancing osteoblast/cementoblast-related gene expression (3,4). Yamamoto and Takahashi (5) reported that epithelial to mesenchymal transformation did not occur in 3 wk-old rats, but their observation is only at one time point, and the developmental stage of teeth in rats is different from that in mice. According to those recent studies, cementoblasts might be derived from dental follicle cells, but not from Hertwig's epithelial root sheath. Besides, some researchers reported that epithelial sheath cells transform into cementoblasts to generate the initial cementum (6–10). The epithelial sheath disintegrates prior to the onset of initial cementogenesis, and a few epithelial cells remain on the root, termed epithelial rests of Malassez. Consequently, the initial cementum forms as an epithelial secretory product (11–15). In contrast, it was observed that stem cells or progenitor cells present in periodontal ligament have the capacity to differentiate into either cementoblastic or osteobalstic cells depending on the microenvironment (16–18). Although a number of studies have been conducted as described above, the origin of cementoblasts is still ambiguous. From the remaining possibilities, we supposed that cementogenesis, which follows epithelial root sheath disruption, might be associated with root formation.

In previous studies, the cementum and periodontal ligament tissue samples were usually obtained by manual curettage under microscopy. It is difficult to isolate pure cementum or periodontal ligament tissues by traditional methods, and those tissues may be contaminated with adjacent tissues, resulting in uncertain outcomes. To address this issue, we have developed laser capture microdissection on non-decalcified frozen sections, which enables us to cut out the target cells under microscopy, and we applied this technique to the present study (19). After extraction of mRNA by the laser capture microdissection system, comparative analyses using a cDNA microarray between mice cementoblasts and periodontal ligament cells and quantitative RT-PCR between mice mandibles and femora were performed to detect the genes related to root morphogenesis (20). Subsequent *in situ* hybridization studies exhibited the specific and temporal expression of *zinc finger helicase* (*ZFH*; 21) in Hertwig's epithelial root sheath during the early stage of root formation. *Zinc finger helicase* is also termed *chromodomain-helicase-DNA-binding protein 3 (Chd3)*, which is known to be a chromatin remodeling factor. This gene encodes a member of the CHD family of proteins, which are characterized by the presence of chromo (chromatin organization modifier) domains and SNF2-related helicase/ATPase domains. Chromatin remodeling is essential for many processes, including transcription, as previously reported (22,23).

Chromodomain-helicase-DNA-binding protein 3 has been regarded as one of the transcriptional regulators and was found in the root-surface cementoblastic cells in our study; however, an association with tooth root development has not yet been reported. Thus, we have tried to elucidate the roles of *Chd3* during root development by demonstrating the gene expression pattern in mouse molars and incisors, in which root extension is terminated by 3 wk of age and not terminated, respectively. Our findings suggest that *Chd3* might play an important role in tooth root development.

Material and methods

Animals and tissue preparation

The day on which a pregnant mouse gave birth was designated as postnatal day (P) 0. Two strains of mice, ICR mice and ddY mice, were purchased from Sankyo Lab Service Corporation (Tokyo, Japan). For *in situ* hybridization, specimens of mandibles of ICR mice (age P7.5, P14.5 and P21.5) were prepared with Leica CM1850 cryostat (Leica Microsystems, Weltzlar, Germany) as described in the following sections. All experimental procedures, which were carried out according to the Guideline for Animal Experimentation at Tokyo Medical and Dental University, were approved (no. 0110230B) by the Animal Welfare Committee of Tokyo Medical and Dental University.

Laser capture microdissection, microarray analysis and quantitative RT-PCR

Microdissection using a PixCell II laser capture system (Arcturus Engineering, Mountain View, CA, USA) was performed as previously reported (19). After microdissection in male 4-wk-old ddY mice, the cell-based samples were extracted, purified, amplified and cRNA labeled using the Two-Cycle cDNA Synthesis kit (Affymetrix Inc., Santa Clara, CA, USA), IVT cRNA amplification kit (MEGA script T7 Kit; Ambion, Inc., Austin, TX, USA) and Two-cycle target labeling assay kit (GeneChip IVT Labeling Kit; Affymetrix Inc.) according to the manufacturer's instructions with some modification.

Postulated cementoblast-specific genes were selected by microarray and quantitative RT-PCR analyses, as previously reported (24). Briefly, 10 μg of biotin-labeled cRNA samples derived from tentative cementum and periodontal ligament cells were hybridized to Affymetrix Mouse 430A 2.0 GeneChip arrays (Affymetrix Inc.). Differentially expressed genes were identified by applying the *S* score algorithm. Probe sets showing absolute values of the S score ≥ 2.00 ($p < 0.05$) were considered to indicate significant differences between the two samples. As the amount of RNA extracted from a laser capture microdissection sample is too small to perform quantitative RT-PCR analysis (Real Time PCR system; Applied Biosystems, Foster City, CA, USA) for various genes, the expression levels of tentative cementoblast-positive and periodontal ligament cell-negative genes in mandibles were compared with the level in femora for the second screening to find the

putative cementoblast-specific genes. The genes that were highly expressed in cementoblasts, among the 2000 genes differentially expressed between cementoblasts and periodontal ligament cells, were sequentially selected, and PCR primers for those genes were designed. Quantitative RT-PCR was performed using mandibles and femora of 4-wk-old male ddY mice as the second screening for cementoblast-specific markers. Subsequently, those which cementoblast-positive/periodontal ligament-negative in microarray and mandible-positive/femur-negative in quantitative RT-PCR were subjected to *in situ* hybridization analysis.

In situ hybridization

Mice mandibles (ICR mice age P7.5, P14.5 and P21.5) were dissected, fixed in 4% paraformaldehyde overnight and decalcified in Morse's solution (10% w/v sodium citrate and 22.5% v/v formic acid) for 1 or 2 d depending on the developmental stage, with moderate stirring at 4°C as previously reported (25). The specimens were then equilibrated in 25% sucrose, embedded in OCT compound (Sakura Finetechnical, Tokyo, Japan) and cut into 10 μm sections. The cutting angle and direction of the frontal and sagittal sections are shown in Fig. 1. The sequence of the primer set for RT-PCR and TA-cloning to prepare cDNA for the Chd3 probe was as follows: forward, GGACGAAATCCTCCCTCT TC and reverse, ATTGGGACAGAC CAGGAGTG. Complementary DNA was transcribed by T3 or T7 RNA polymerase to prepare a digoxygenin-labeled RNA probe for *ZFH/Chd3*, and the probe size was reduced to an average of 250 bases by alkaline hydrolysis. *In situ* hybridization was carried out using an automated system in a hybridization machine (Hybrimaster HS-300; Aloka, Tokyo, Japan) as previously reported (26,27). Signals were visualized with nitroblue phosphate /5-bromo,4-chloro,3-indolil phosphate (NBT/BCIP; Roche Diagnostics Corporation, Indianapolis, IN, USA). Sense probe was used to distinguish the positive signals from nonspecific binding. All results shown are representative of multiple independent experiments.

Results

Laser capture microdissection, microarray analysis and quantitative RT-PCR

More than 500 tentative cementoblasts and periodontal ligament cells in the nondecalcified frozen sections of 4-wk-old male ddY mice were successfully laser captured under microscopy. The total amount of RNA extracted from laser capture microdissection samples was <1 μg; however, the quality was considerably high, showing clear peaks of 18S and 28S rRNA. Subsequent cDNA microarray analysis revealed that approximately 2000 out of 39,000 genes were differentially expressed between the cementoblasts and the periodontal ligament cells, as we have previously reported (20). Among those, *ZFH* (GeneBank/EMBL accession no. AK011183, NCBI Gene ID: 10264) was one of the putative cementoblast-positive and periodontal ligament cell-negative genes. Real-time PCR revealed that the expression level of *ZFH* in mandible was higher than that in femur. The record of *ZFH* was replaced with Gene ID: 1107 and thereafter termed *Chd3*. Notably, the expression level of *ZFH/Chd3* in mandible was approximately 10 times higher than in femur (20). It might be possible that this gene could play some roles in cementogenesis, root formation or root elongation, and *in situ* hybridization analysis was conducted in developing molars and incisors.

Localization of Chd3 during root formation

In situ hybridization studies in developing ICR mice mandible revealed that *Chd3* was strongly expressed in the cells that formed Hertwig's epithelial root sheath in the first molar at P7.5, the initial stage of root formation, during which Hertwig's epithelial root sheath had been formed by inner and outer enamel epithelial cells [Fig. 2A and B (arrows)]. In addition, its expression was detected in differentiating ameloblasts arranged on the extended line of inner enamel epithelium. Although *Chd3* was picked up from the cementoblast-positive and mandible-specific sample, *Chd3*-positive cells were abundantly contained by the cells organizing Hertwig's epithelial root sheath rather than by cementoblasts, which are scarcely observed at this stage. In contrast, dental pulp or differentiating periodontal ligament fibroblasts from molars did not express *Chd3* transcript (Fig. 2B). At P7.5, *Chd3* expression was also observed in ameloblasts located to the labial side of incisors, as shown in Fig. 2A and C (arrowheads), but not in dental pulp (Fig. 2C). Expression of *Chd3* was scarcely observed in the stellate reticulum and the duct epithelium of salivary glands (data not shown).

The frontal sections of P14.5 mandibles, at the developmental stage of root elongation, demonstrated that mRNA expression of *Chd3* was prominent along the enamel epithelium at the tip of the developing first molar root (Fig. 3A). *Chd3* solidly positive

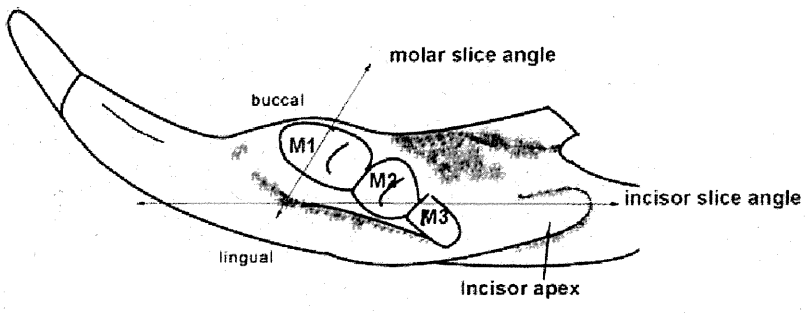

Fig. 1. Slice angle and direction in the mandible.

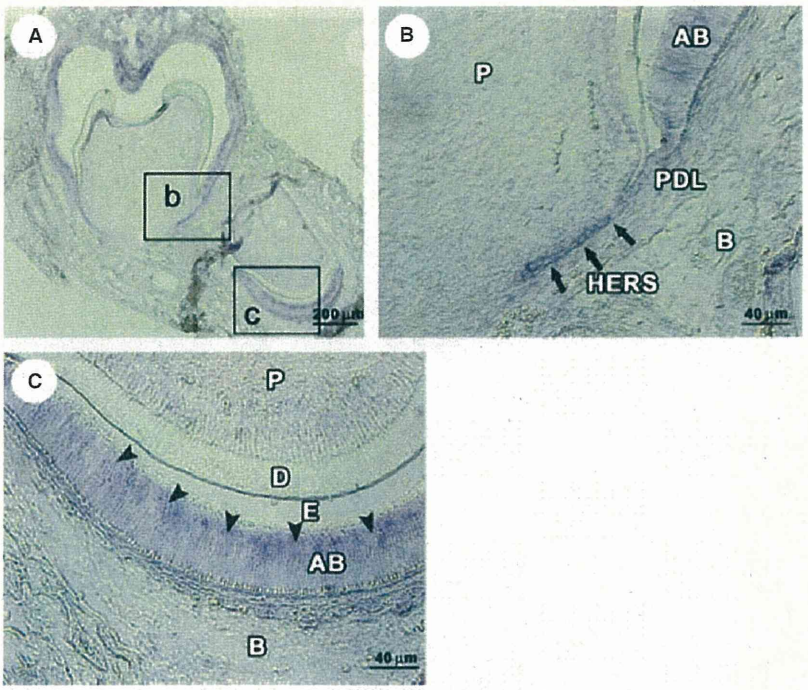

Fig. 2. Expression of Chd3 in the developing lower first molar at P7.5. (A) Chd3 expression in a frontal section of the mandibular first molar of a P7.5 mouse assessed by *in situ* hybridization. (B) A higher magnification of the apex of the molar root. Chd3 was expressed in Hertwig's epithelial root sheath (arrows), but was absent in the dental pulp and periodontal ligament. (C) A higher magnification of the labial side of the incisor. Chd3 was expressed in ameloblasts of the incisor (arrowheads), but not in dental pulp. Abbreviations: AB, ameloblast; B, bone; D, dentin; E, enamel; HERS, Hertwig's epithelial root sheath; P, dental pulp; and PDL, periodontal ligament. All results shown are representative of multiple independent experiments.

structures were restricted to the monolayer at both ends of Hertwig's epithelial root sheath, with weakly positive areas in the dental pulp (Fig. 3B, arrows). No signal was detected in periodontal ligament fibroblasts adjacent to the molar root. Similar to P7.5 mandible, *Chd3* expression was observed in ameloblasts on the labial side of incisors (Fig. 3C, arrowheads).

At the advanced stage of root formation, P21.5, the first molar was almost completely developed and a definitive Hertwig's epithelial root sheath structure was mostly collapsed, whereas the incisor root was continuously extending. At this time point, in contrast to P7.5 or P14.5, the expression level of *Chd3* in Hertwig's epithelial root sheath was significantly reduced to the background level at the tip of the first molar roots (Fig. 4B, arrows). Its expression was absent in periodontal ligament (Fig. 4B). Similar to molars, *Chd3* signal was scarcely detected in ameloblasts at the labial side of incisors (Fig. 4C, arrowheads).

Regarding incisor roots, the root extension is not terminated and the original structure of cervical loop is preserved at P7.5, P14.5 and P21.5. As shown in Fig. 5, *in situ* hybridization analysis of the sagittal section of the developing incisors from P7.5 to P21.5 demonstrated specific and apparent localization of *Chd3*. In the inner and outer epithelium of the labial side of incisors, Chd3 was abundantly expressed, and its expression level was maintained with the looped shape of epithelial cells throughout the observation period.

Discussion

In the present study, a number of prospective cementoblast-specific genes derived from cementum-positive, periodontal ligament-negative and mandible-positive, femora-negative samples were identified. Of these genes, as a predictable cementoblast-specific gene, *ZFH/Chd3* was intensively investigated. Indeed, *ZFH/Chd3* was strongly expressed in the cells at the apical end of the tooth root, as shown in Figs 2 and 3. Notably, the positive signal was highly specific in the pointed end of Hertwig's epithelial root sheath and epithelial diaphragm in P7.5 and P14.5 mouse mandibles, in which few cementoblasts appeared on the root. These results suggest that this molecule is highly specific for Hertwig's epithelial root sheath rather than cementum. *Chd3* is one of the components of a histone deacetylase complex referred to as the Mi-2/NuRD complex, which participates in the remodeling of chromatin by deacetylating histones (22,23). Abundant *Chd3* expression in the apical root end at the developmental stage of root formation could be reasonable because *Chd3* is a chromatin remodeling associated factor, and the cells organizing Hertwig's epithelial root sheath are actively remodeled to extend the tooth root. It is

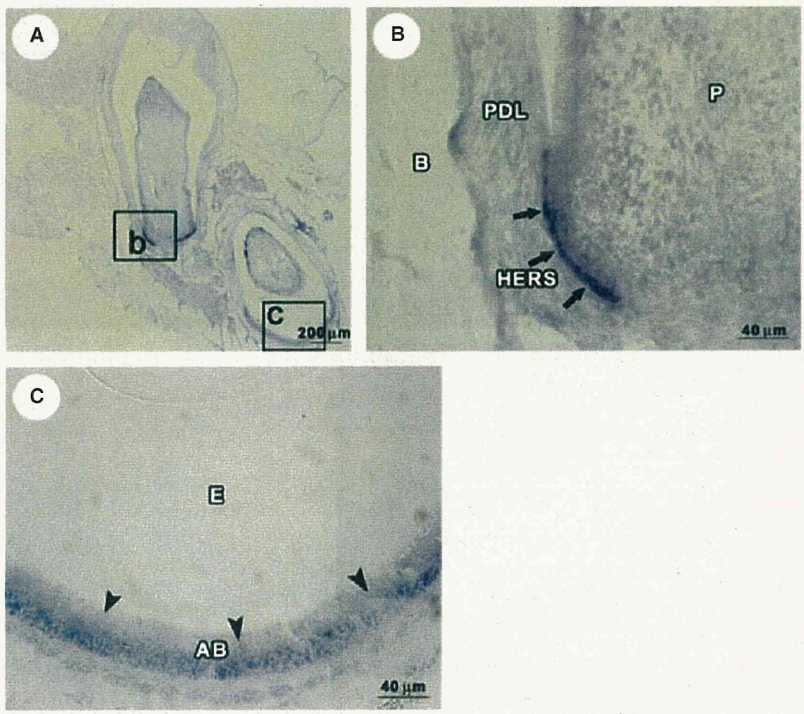

Fig. 3. Expression of Chd3 in the developing lower first molar at P14.5. (A) Chd3 expression in a frontal section of the mandibular first molar of a P14.5 mouse assessed by *in situ* hybridization. (B) A higher magnification of the apex of the molar root. Chd3 was strongly expressed in Hertwig's epithelial root sheath (arrows) and weakly in the dental pulp, but was absent in periodontal ligament. (C) A higher magnification of the labial side of the incisor. Chd3 was expressed in ameloblasts of the incisor (arrowheads). Abbreviations: AB, ameloblast; B, bone; D, dentin; E, enamel; HERS, Hertwig's epithelial root sheath; P, dental pulp; and PDL, periodontal ligament. All results shown are representative of multiple independent experiments.

generally accepted that Hertwig's epithelial root sheath is the principal region controlling root extension, because Hertwig's epithelial root sheath usually disappears upon the completion of root formation. Previously, several researchers described that, during cementogenesis, dental follicle cells differentiate into cementoblasts, or Hertwig's epithelial root sheath cells transform and then become functional cementoblasts (1,2). As our experiments revealed intensive expression of *Chd3* in Hertwig's epithelial root sheath, it might be an important factor not only for root extension but also for initiation of cementogenesis.

As mentioned above, there was restricted expression of *Chd3* on the molar root. However, there was a contradiction between the results of the Genechip analysis with quantitative RT-PCR and those of *in situ* hybridization. In 4 wk-old ddY mice, significantly intense expression of *Chd3* was shown in cementoblasts or mandible by Genechip analysis or quantitative RT-PCR, respectively. In contrast, this positive expression in Hertwig's epithelial root sheath of molars was not so apparent at 3 wk (P21.5) by *in situ* hybridization. *Chd3* expression in cementoblasts was assumed to be extremely low, and amplification might be required to detect it. In our preliminary experiment, another set of quantitative PCR results from laser capture microdissection samples confirmed that *Chd3* expression in the cementum layer was more than three times as high as that in the periodontal ligament region (data not shown). Moreover, expression of *Chd3* could not be observed in tentative cementoblasts or in periodontal ligament cells with lower cycle amplification (< 20 cycles) in the PCR, suggesting a low level of expression in cementoblasts, but higher than in other tissues of the periodontium at 4 wk. Another possible explanation is that a laser capture microdissection sample derived from tentative cementoblasts may include cells of Hertwig's epithelial root sheath or epithelial rests of Malassez. As laser capture microdissection was carried out on the root surface of nondecalcified frozen sections, it seemed to be difficult, even under the microscope, to eliminate the epithelial rests if they exist.

To confirm the role of *Chd3*, its expression around the molar roots was compared with that around the apex of incisor roots, where characteristic and continuous root extension is observed. As restricted *Chd3* expression was observed on the molar roots during the root extension period, it was very interesting to investigate how *Chd3* behaves in the case of continuous root extension. Morphological features of rodent incisors are quite characteristic. The cells on the lingual side usually develop only to the pre-ameloblastic stage, and no enamel is produced. In

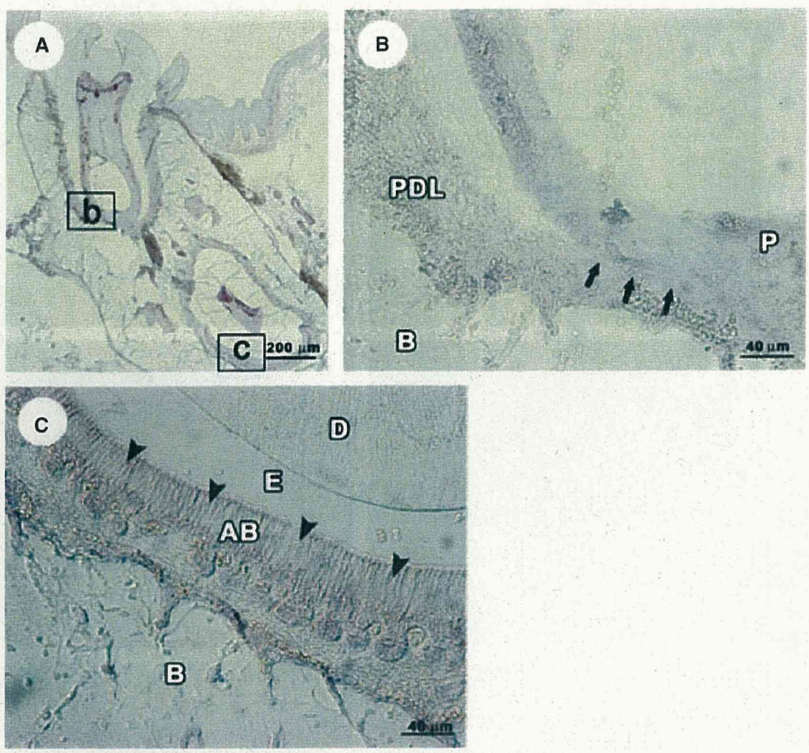

Fig. 4. Expression of Chd3 in the developing lower first molar at P21.5. (A) Chd3 expression in a frontal section of the mandibular first molar of a P21.5 mouse assessed by *in situ* hybridization. (B) A higher magnification of the apex of the molar root. Chd3 was scarcely expressed in Hertwig's epithelial root sheath (arrows) and the dental pulp. It was absent in periodontal ligament. (C) A higher magnification of the labial side of the incisor. Chd3 was barely expressed in ameloblasts of the incisor (arrowheads). Abbreviations: AB, ameloblast; B, bone; D, dentin; E, enamel; HERS, Hertwig's epithelial root sheath; P, dental pulp; and PDL, periodontal ligament. All results shown are representative of multiple experiments.

contrast, on the labial side of the cervical loop, the cells of the inner enamel epithelium continuously develop dental organs, and root extension is never terminated (28,29). In the specimen of incisors, *Chd3* was expressed in the cells organizing the cervical loop throughout the observation period. In particular, along the inner enamel epithelium and around the apical bud, intensive expression was observed where apical root extension was maintained owing to the continuous incisor eruption. From these results, we propose that the restricted expression of *Chd3* plays an important role for epithelial cell progression in root morphogenesis and that termination of *Chd3* expression might be crucial for cementogenesis. In addition, the expression pattern of *Chd3* was different from other amelobalstic markers, such as sonic hedgehog, in that the expression was remarkably distinctive along the inner enamel epithelium (data not shown). Moreover, the observation of continuous *Chd3* expression in the cells of the cervical loop of incisors at 3 wk, while little expression was observed in molars, also supports a contribution of *Chd3* to the apical extension of the tooth root. However, another ambiguous point remains. Intensive expression of *Chd3* was always detected in Hertwig's epithelial root sheath, whereas it was not always obvious in other areas, such as odontoblasts, stellate reticulum or stratum intermedium. We cannot clearly explain this unstable detection of *Chd3* except in Hertwig's epithelial root sheath area. A possible explanation is that *Chd3* expression is stage dependent and that the unstable detection might be due to a pause in growth. Another possible explanation is that *Chd3* is also a component of a histone deacetylase complex, referred as the Mi-2/NuRD complex, participating in the remodeling of chromatin by deacetylating histones and then *Chd3* could regulate the transcription process. Unstable detection of *Chd3*, in which cells dynamically and drastically transform depending on developmental stages, might be reasonable (23). Of course, the possibility of a false positive has not been ruled out, and we may have to improve the histological technique considerably.

In conclusion, *Chd3* was expressed at the epithelial diaphragm from P7.5 to P21.5, and the signal faded from Hertwig's epithelial root sheath with progression of root formation. At 3 wk, *Chd3* expression was hardly detectable in the molar root. These results suggest that restricted expression of *Chd3* in Hertwig's epithelial root sheath should be tightly correlated to the apical root morphogenesis. Although further functional analysis, such as employing transgenic animals or siRNA knock-down analysis, is required to confirm the fundamental

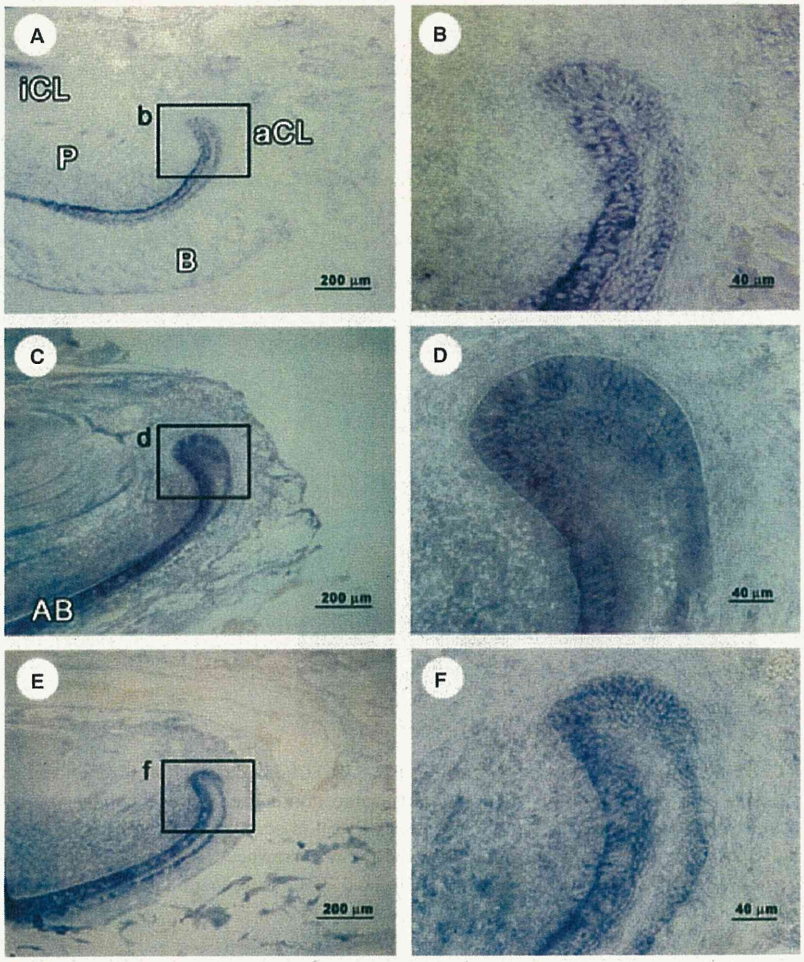

Fig. 5. Localization of Chd3 in the developing incisor from P7.5 to P21.5. The samples are sagittal sections in the developing lower incisors from P7.5 to P21.5. (B), (D) and (F) are higher magnification images of the boxes in (A), (C) and (E), respectively. Chd3 was strongly expressed in the inner and outer enamel epithelium of the labial cervical loop. Abbreviations: AB, ameloblast; aCL, labial cervical loop; B, bone; iCL, lingual cervical loop; and P, dental pulp. All results shown are representative of multiple independent experiments.

function, *Chd3* might contribute to the initiation and termination of apical root extension and might be an essential molecule to induce cementogenesis, which follows Hertwig's epithelial root sheath disruption. *Chd3* might have a possible therapeutic use for regeneration of periodontal tissue. This is the first report to describe the expression of chromatin remodeling factor *Chd3* in tooth root development.

Acknowledgements

We would like to thank Dr Teerasak Damrongrungruang (Khonkaen University) and Ms Michiko Suzuki (Tokyo Medical and dental University) for technical assistance. This work was supported by Grants-in-Aid from the Japanese Society for the Promotion of Science (nos 14657551 and 16689034) and the Japanese Ministry of Education [Global (21st Century) Center of Excellence (COE) Program, International Research Center for Molecular Science in Tooth and Bone Diseases, nos 18109011, 18659438, 18123456 and 20013014].

References

1. Bosshardt DD, Nanci A. Immunolocalization of epithelial and mesenchymal matrix constituents in association with inner enamel epithelial cells. *J Histochem Cytochem* 1998;**46:**135–142.
2. Lezot F, Davideau JL, Thomas B, Sharpe P, Forest N, Berdal A. Epithelial Dlx-2 homeogene expression and cementogenesis. *J Histochem Cytochem* 2000;**48:**277–284.
3. Diekwisch TG. The developmental biology of cementum. *Int J Dev Biol* 2001; **45:**695–706.
4. Pan K, Sun Q, Zhang J *et al.* Multilineage differentiation of dental follicle cells and the roles of Runx2 over-expression in enhancing osteoblast/cementoblast-related gene expression in dental follicle cells. *Cell Prolif* 2010;**43:**219–228.
5. Yamamoto T, Takahashi S. Hertwig's epithelial root sheath cells do not transform into cementoblasts in rat molar cementogenesis. *Ann Anat* 2009;**191:**547–555.
6. Thomas HF. Root formation. *Int J Dev Biol* 1995;**39:**231–237.
7. Bosshardt DD, Nanci A. Immunodetection of enamel- and cementum-related (bone) proteins at the enamel-free area and cervical portion of the tooth in rat molars. *J Bone Miner Res* 1997;**12:**367–379.
8. Bosshardt DD, Zalzal S, McKee MD, Nanci A. Developmental appearance and

distribution of bone sialoprotein and osteopontin in human and rat cementum. *Anat Rec* 1998;**250:**13–33.
9. Zeichner-David M, Oishi K, Su Z *et al.* Role of Hertwig's epithelial root sheath cells in tooth root development. *Dev Dyn* 2003;**228:**651–663.
10. Bosshardt DD. Are cementum a subpopulation of osteoblasts or a unique phenotype? *J Dent Res* 2005;**84:**390–406.
11. Paynter KJ, Pudy G. A study of the structure, chemical nature, and development of cementum in the rat. *Anat Rec* 1958;**131:**233–251.
12. Owens PD. A light and electron microscopic study of the early stages of root surface formation in molar teeth in the rat. *Arch Oral Biol* 1979;**24:**901–907.
13. Slavkin HC, Bessem C, Fincham AG *et al.* Human and mouse cementum proteins immunologically related to enamel proteins. *Biochim Biophys Acta* 1989;**991:**12–18.
14. Hammarstrom L, Alatli I, Fong CD. Origins of cementum. *Oral Dis* 1996;**2:**63–69.
15. Hammarstrom L. Enamel matrix, cementum development and regeneration. *J Clin Periodontol* 1997;**24:**658–668.
16. Isaka J, Ohazama A, Kobayashi M *et al.* Participation of periodontal ligament cells with regeneration of alveolar bone. *J Periodontol* 2001;**72:**314–323.
17. Shimono M, Ishikawa T, Ishikawa H *et al.* Regulatory mechanisms of periodontal regeneration. *Microsc Res Tech* 2003;**60:**491–502.
18. Seo BM, Miura M, Gronthos S *et al.* Investigation of multipotent postnatal stem cells from human periodontal ligament. *Lancet* 2004;**364:**149–155.
19. Yokoyama Y, Damrongrungruang T, Suzuki M *et al.* Application of laser capture microdissection to periodontal tissue. *J Oral Tissue Engin* 2007;**4:**155–160.
20. Yokoyama Y. Comparison of gene expression of profile of cementoblasts with periodontal ligament cells in mouse mandible with laser capture microdissection. *Kokubyo Gakkai Zasshi* 2008;**75:**13–28.
21. Aubry F, Mattei MG, Galibert F. Identification of a human 17p-located cDNA encoding a protein of the Snf2-like helicase family. *Eur J Biochem* 1998;**254:**558–564.
22. Woodage T, Basrai MA, Baxevanis AD, Hieter P, Collins FS. Characterization of the CHD family of proteins. *Proc Natl Acad Sci U S A* 1997;**94:**11472–11477.
23. Ge Q, Nilasena DS, O'Brien CA, Frank MB, Targoff IN. Molecular analysis of a major antigenic region of the 240-kD protein of Mi-2 autoantigen. *J Clin Invest* 1995;**96:**1730–1737.
24. Yokoyama Y, Damrongrungruang T, Kuroda S *et al.* Comparative analysis of gene expression by cDNA microarray between cementoblasts and periodontal ligament cells in the murine mandible. *J Oral Biosci* 2008;**50:**183–193.
25. Nakatomi M, Morita I, Eto K, Ota MS. Sonic hedgehog signaling is important in tooth root development. *J Dent Res* 2006;**85:**427–431.
26. Iseki S, Wilkie AO, Morriss-Kay GM. Fgfr1 and Fgfr2 have distinct differentiation- and proliferation-related roles in the developing mouse skull vault. *Development* 1999;**126:**5611–5620.
27. Xu Q, Wilkinson DG. *In situ* hybridization of mRNA with hapten labelled probes. In: Wilkinson DG, ed. *In situ Hybridization: a Practical Approach*, 2nd edition. Oxford: Oxford University Press 1999:87–106.
28. Mellanby H. The development of teeth in the Albino rat. *Br Dent J* 1939;**66:**76–86.
29. Josephsen K, Takano Y, Frische S *et al.* Ion transporters in secretory and cyclically modulating ameloblasts: a new hypothesis for cellular control of preeruptive enamel maturation. *Am J Physiol Cell Physiol* 2010;**299:**C1299–C1307.

OPEN ACCESS Freely available online

PLoS one

Functional Tooth Regeneration Using a Bioengineered Tooth Unit as a Mature Organ Replacement Regenerative Therapy

Masamitsu Oshima[1☯], Mitsumasa Mizuno[1,2☯], Aya Imamura[3], Miho Ogawa[1,4], Masato Yasukawa[3], Hiromichi Yamazaki[3], Ritsuko Morita[1], Etsuko Ikeda[2], Kazuhisa Nakao[1], Teruko Takano-Yamamoto[2], Shohei Kasugai[5], Masahiro Saito[1,3], Takashi Tsuji[1,3,4]*

1 Research Institute for Science and Technology, Tokyo University of Science, Noda, Chiba, Japan, **2** Division of Orthodontics and Dentofacial Orthopedics, Graduate School of Dentistry, Tohoku University, Sendai, Miyagi, Japan, **3** Department of Biological Science and Technology, Graduate School of Industrial Science and Technology, Tokyo University of Science, Noda, Chiba, Japan, **4** Organ Technologies Inc., Tokyo, Japan, **5** Oral Implantology and Regenerative Dental Medicine Graduate School, Tokyo Medical and Dental University, Bunkyo-ku, Tokyo, Japan

Abstract

Donor organ transplantation is currently an essential therapeutic approach to the replacement of a dysfunctional organ as a result of disease, injury or aging *in vivo*. Recent progress in the area of regenerative therapy has the potential to lead to bioengineered mature organ replacement in the future. In this proof of concept study, we here report a further development in this regard in which a bioengineered tooth unit comprising mature tooth, periodontal ligament and alveolar bone, was successfully transplanted into a properly-sized bony hole in the alveolar bone through bone integration by recipient bone remodeling in a murine transplantation model system. The bioengineered tooth unit restored enough the alveolar bone in a vertical direction into an extensive bone defect of murine lower jaw. Engrafted bioengineered tooth displayed physiological tooth functions such as mastication, periodontal ligament function for bone remodeling and responsiveness to noxious stimulations. This study thus represents a substantial advance and demonstrates the real potential for bioengineered mature organ replacement as a next generation regenerative therapy.

Citation: Oshima M, Mizuno M, Imamura A, Ogawa M, Yasukawa M, et al. (2011) Functional Tooth Regeneration Using a Bioengineered Tooth Unit as a Mature Organ Replacement Regenerative Therapy. PLoS ONE 6(7): e21531. doi:10.1371/journal.pone.0021531

Editor: Wei-Chun Chin, University of California, Merced, United States of America

Received April 8, 2011; **Accepted** May 30, 2011; **Published** July 12, 2011

Funding: This work was partially supported by Health and Labour Sciences Research Grants from the Ministry of Health, Labour, and Welfare (No. 21040101) to T.T., a Grant-in Aid for Scientific Research in Priority Areas (No. 50339131) to T.T., a Grant-in-Aid for Scientific Research (A) to T.T. and a Grant-in-Aid for Young Scientists (B) to M. Oshima from Ministry of Education, Culture, Sports and Technology, Japan. The funders had no role in study design, data collection and analysis, decision to publish, or preparation of the manuscript.

Competing Interests: The authors have declared that no competing interests exist.

* E-mail: t-tsuji@rs.noda.tus.ac.jp

☯ These authors contributed equally to this work.

Introduction

Donor organ transplantation is currently essential to replace a dysfunctional organ and to restore organ function *in vivo* [1,2]. This approach is problematic for clinicians however as donor organs are constantly in short supply [2,3]. An attractive new concept in current regenerative therapy that may possibly replace conventional transplantation in the future is stem cell transplantation therapy [4,5] or a two-dimensional uniform cell sheet technique [6,7] to repair the local sites of the damaged tissues and organs [8]. The ultimate goal of regenerative therapy in the future is to develop organ replacement regenerative therapies that will restore lost or damaged tissues following disease, injury, or aging with a fully functioning bioengineered organ [9,10,11]. To construct a bioengineered organ, one of two major concepts is to construct fully functional artificial organs using three-dimensional tissue-engineering technology, involving biodegradable materials and various cell types, that can immediately function after transplantation *in vivo* [12,13,14]. However, further technological developments are required to create such artificial organs which can immediately function [15].

For the regeneration of ectodermal organs such as a tooth, hair follicle or salivary gland [16,17], a further concept has been proposed in which a bioengineered organ is developed from bioengineered organ germ by reproducing the developmental processes that take place during organogenesis [11,18]. Tooth regenerative therapy is thought to be a very useful study model for organ replacement therapies [11,19,20]. The loss of a tooth causes fundamental problems in terms of oral functions, which are achieved in harmony with the teeth, masticatory muscles and the temporomandibular joint under the control of the central nervous system [21]. It has been anticipated that a bioengineered tooth could restore oral and physiological tooth functions [19]. We have previously developed a three-dimensional cell manipulation method, designated the organ germ method, for the reconstitution of bioengineered organ germ, such as a tooth or whisker follicle [22]. This bioengineered tooth erupted with the correct structure, occluded at the lost tooth region in an adult mouse. It also showed sufficient masticatory performance, periodontal functions for bone remodeling and the proper responsiveness to noxious stimulations [20]. This previous study thus provided a proof of concept that

successful replacement of an entire and fully functioning organ could be achieved through the transplantation of bioengineered organ germ i.e. a successful organ replacement regenerative therapy [20].

Transplantation of a bioengineered mature organ will lead to immediately perform of the full functions *in vivo* and have a profound impact on the survival outcomes of many diseases [2,9]. Transplanted bioengineered organs are also expected to be viable over the long-term and achieve the continuous production of various functional cells and their progenitors from stem cells as efficiently as the natural organ *in vivo* [23,24]. It has also been proposed that mature organs can be developed from bioengineered organ germ by faithfully reproducing *in vivo* developmental processes. In the dental treatment, it has been expected to transplant of a bioengineered tooth unit comprising mature tooth, periodontal ligament (PDL) and alveolar bone into the tooth loss region through bone integration, which is connected between recipient bone and bioengineered alveolar bone in a bioengineered tooth unit [25]. Transplantation of a bioengineered tooth unit has also been proposed as a viable option to repair the large resorption defects in the alveolar bone after tooth loss [26]. However, there are currently no published reports describing successful transplantation or replacement using a bioengineered tooth [10,27].

In our current study, we have generated a bioengineered tooth unit, which was controlled for length and shape and report a successful tooth replacement by transplantation of a bioengineered tooth unit into the tooth loss region, followed by successful bone integration, and restoration of tooth physiological functions such as mastication, PDL function and an appropriate responsiveness to noxious stimulations. This transplantation of a bioengineered tooth unit could also regenerate alveolar bone formation in a vertical direction. Our results thus further demonstrate the potential for bioengineered tooth replacement as a future regenerative therapy.

Results

Generation of a Bioengineered Tooth Unit

We have previously reported that bioengineered tooth germ can successfully develop a bioengineered tooth that by subrenal capsule transplantation can restore a mature tooth, including periodontal tissue and alveolar bone [22]. Because a three-dimensional *in vitro* organ culture has not yet been developed, we employed a strategy involving a bioengineered tooth unit, which has the necessary tissues to restore tooth functions, to investigation and advance the future potential of bioengineered tooth replacement (figure 1A). The bioengineered molar tooth germ was developed to a stage equivalent to the early bell stage of natural tooth germ for 5–7 days in an *in vitro* organ culture (figure 1B). Although we have previously reported that multiple bioengineered teeth have been formed from a bioengineered tooth germ reconstituted by our organ germ method [22], we recently developed a method to generate a single and width-controlled bioengineered tooth [28]. The bioengineered tooth germ gradually accumulated hard tissue, root extension, and an increased alveolar bone volume, depending on transplantation periods, and could successfully generate a tooth unit with the correct structure of a whole molar, and the proper formation of periodontal tissue and surrounding alveolar bone (figure 1C, D). However, the shape (x vs. y axis) of the bioengineered tooth unit was flattened by the pressure of the outer membrane of the subrenal capsule (figure 1F, G). The length of the tooth also showed continuous root elongation depending on the transplantation periods without occlusional mechanical stress (figure 1C, F, H).

To generate the shape- and length-controlled bioengineered tooth unit so that a suitable size was obtained for intraoral transplantation, the tooth germ was inserted into a ring-shaped size-control device and then transplanted into a subrenal capsule (figure 1E). The crown widths, calculated from the x/y axis ratios, of natural first, second and third molars of 9-week-old adult mice were 1.61 ± 0.05 mm, 1.09 ± 0.04 mm, 1.12 ± 0.04 mm, respectively (each $n = 5$, figure 1G). The crown width of the bioengineered tooth units grown in the size-control device, which had a 1.8 mm inside diameter and 1.3 mm thickness, was 1.46 ± 0.16 mm whereas when grown outside of the device the size was 2.30 ± 0.35 mm (each $n = 5$, figure 1G). The device thus successfully generated a size-controlled bioengineered tooth so that it was similar to a natural tooth (figure 1F, G). This device could avoid the pressure by the subrenal capsule membrane, and reserve the three-dimensional space for developing a bioengineered tooth germ normally. We next evaluated the length of a bioengineered tooth unit generated in the size-control device (figure 1E). After 30 or 60 days, the lengths of the teeth transplanted without the devices were 1.07 ± 0.20 mm and 1.70 ± 0.26 mm, respectively, which was significantly associated with the transplantation period (each $n = 5$, figure 1H, figure S1A). Although the length of the bioengineered tooth transplanted without the devices was 1.70 ± 0.26 mm after 60 days transplantation, bioengineered teeth transplanted in devices of 1.3 or 1.8 mm in diameter, was significantly regulated at 1.02 ± 0.11 or 1.27 ± 0.06 mm, respectively (each $n = 5$, figure 1H). The shape and length of the bioengineered tooth unit can therefore be controlled in three-dimensions using a specialized device.

Multiple bioengineered tooth units surrounded by alveolar bone could be also generated by the transplantation of several tooth germs into a single size-control device (figure 1I, figure S1B). Each resulting tooth had the correct structure including pulp cavities and partitioned periodontal spaces (figure 1I, figure S1C). Hence, multiple tooth replacements can be achieved with this regenerative transplantation method.

Transplantation of a Bioengineered Tooth Unit into a Tooth Loss Region *in Vivo*

We next investigated whether a bioengineered tooth unit could be engrafted via the integration between the alveolar bone of this unit and that of the host recipient and then function appropriately by occlusion with an opposing tooth (figure 2A). The bioengineered tooth unit, which was generated by transplantation in a device of a 2.5 mm inside diameter for 50–60 days and labeled by the administration of calcein reagent into recipient mouse (figure 2B), was transplanted with the correct orientation into a properly-sized bony hole in the lower first molar region of the alveolar bone in a 4-week-old mouse (figure 2C). Briefly, in this mouse model, the lower first molar had been extracted, and the resulting gingival wounds had been allowed to heal for 4–6 days (figure S2A). When the bioengineered tooth unit was transplanted, it was located at a position reaching the occlusal plane with the opposing upper first molar (figure 2C, figure S2A). Partial bone integration was observed at 14 days after transplantation, and full bone integration around a bioengineered tooth root was seen at 30 days after transplantation (figure 2C). In the calcein-labeled alveolar bone of bioengineered tooth unit, resorption was partially observed at the surface at 30 days post-transplantation (figure 2D, figure S2B). The calcein-labeled bone finally disappeared and the recipient bone around the bioengineered tooth root replaced it completely at 40 days after transplantation at a frequency of 66/83 (79.5%; figure 2C, D, figure S2B). There have been many previously reported clinical cases of multiple tooth loss, the most serious condition being edentulism [29]. It is possible that a

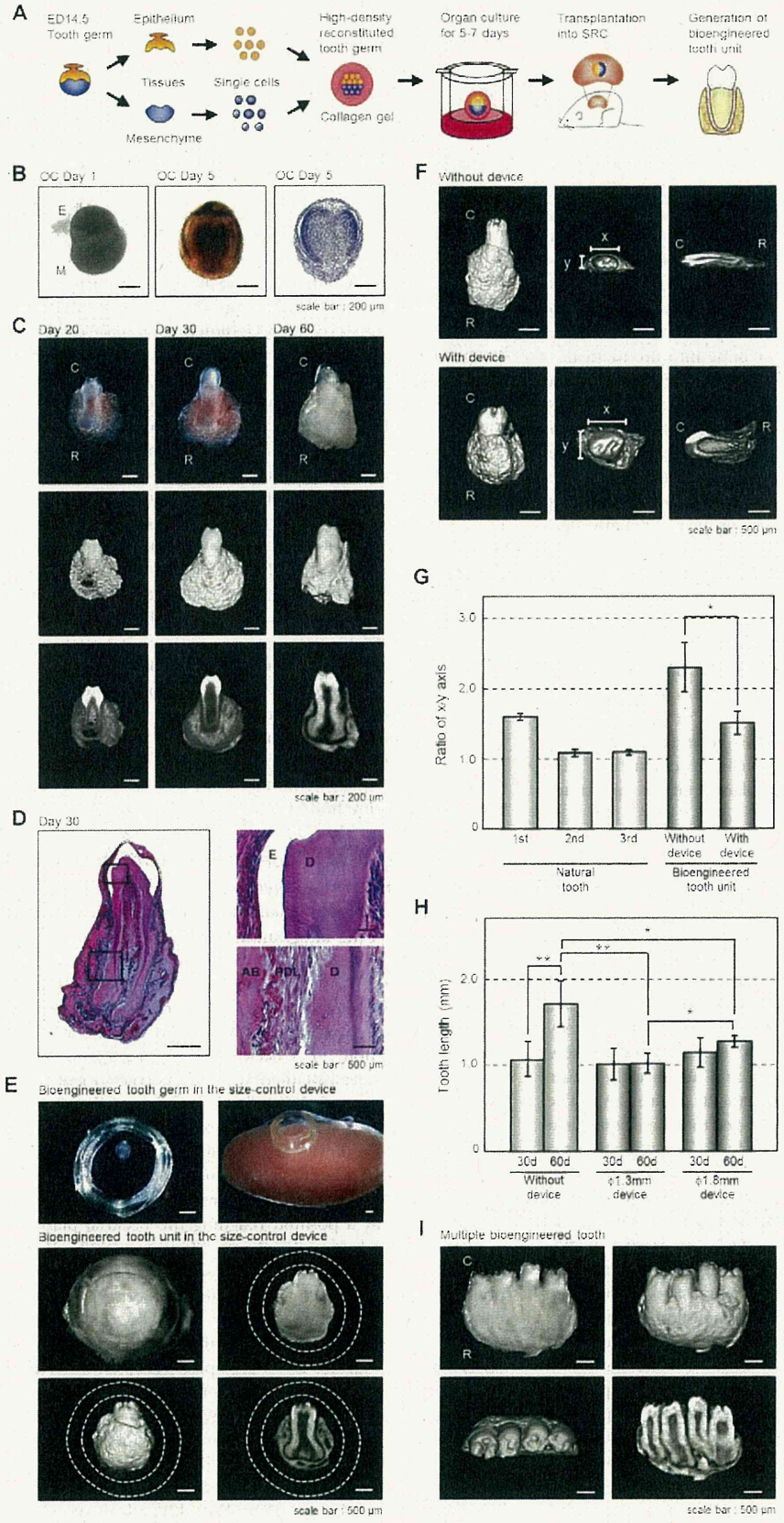
A
ED14.5 Tooth germ
Epithelium
Tissues
Mesenchyme
Single cells
High-density reconstituted tooth germ
Collagen gel
Organ culture for 5-7 days
Transplantation into SRC
Generation of bioengineered tooth unit
B
OC Day 1
OC Day 5
OC Day 5
E
M
scale bar : 200 μm
C
Day 20
Day 30
Day 60
C
R
scale bar : 200 μm
D
Day 30
E
D
AB
PDL
D
scale bar : 500 μm
E
Bioengineered tooth germ in the size-control device
Bioengineered tooth unit in the size-control device
scale bar : 500 μm
F
Without device
With device
C
R
X
Y
scale bar : 500 μm
G
Ratio of x/y axis
3.0
2.0
1.0
0
1st
2nd
3rd
Without device
With device
Natural tooth
Bioengineered tooth unit
H
Tooth length (mm)
2.0
1.0
0
30d
60d
Without device
φ1.3mm device
φ1.8mm device
I
Multiple bioengineered tooth
C
R
scale bar : 500 μm

Figure 1. Generation of a bioengineered tooth unit. (A) Schematic representation of the generative technology of bioengineered tooth unit. (B) Phase construct imagery of a bioengineered tooth germ on day 1 (*left*) and 5 (*center*) and HE staining (*right*) of an organ culture on day 5. Scale bar, 200 μm. E, epithelium; M, mesenchyme. (C) Photographs (*upper*) and micro-CT images of the external surface area (*middle*) and cross section (*lower*) of a bioengineered tooth unit. Images were captured at 20 days (*left*), 30 days (*center*) and 60 days (*right*) after subrenal capsule transplantation (SRC). Scale bar, 200 μm. C, tooth crown side; R, tooth root side. (D) Histological analysis of the bioengineered tooth unit on day 30 after SRC transplantation (*left*). (Scale bar, 500 μm). Higher magnification images of crown area (*upper right*) and the periodontal tissue area (*lower right*) are also shown. Scale bar, 50 μm. E, enamel; D, dentin; AB, alveolar bone; PDL, periodontal ligament. (E) Photographs of the developmental processes occurring in bioengineered tooth germ in a subrenal capsule (SRC) using a size-control device. Images were captured of bioengineered tooth germ orientated in the device (*top left*), transplantation into the SRC (*top right*), and the bioengineered tooth at 50–60 days after transplantation in the SRC (middle). Micro-CT images of the external surface area (*bottom left*) and cross section (*bottom left*) are also show. The dotted lines indicate the outlines of the device. Scale bar, 500 μm. (F) Micro-CT images of a bioengineered tooth unit transplanted into the SRC for 30 days with (*lower column*) or without (*upper column*) the size-control device at an external (*left*), axial (*center*) or cross section (*right*) view. Scale bar, 500 μm. x, x-axis of the crown; y, y-axis of the crown. (G) X-axis versus y-axis ratios (x/y) of the crowns of bioengineered tooth units at 30 days post transplantation into an SRC, and also of natural first, second and third molars from 9-week-old mice. Transplantations were performed with or without the 1.3 mm thickness size-control device. Error bars show the standard deviation ($n=5$). *$P<0.001$ (*t*-test). (H) The lengths of the bioengineered tooth units generated using size-control devices, which were of a 1.3 mm (φ1.3 mm) or 1.8 mm (φ1.8 mm) inner diameter, at 30 and 60 days post transplantation into an SRC were compared with or without the devices. Error bars show the standard deviation ($n=5$). *$P<0.01$ and **$P<0.001$ (*t*-test). (I) Photograph (*first figure from the left*) and micro-CT images showing external (*second figure*), axial (*third figure*) and cross section (*fourth figure*) views of a multiple bioengineered tooth units, in which four teeth were contained in one alveolar bone, after 60 days transplantation into the SRC. Scale bar, 500 μm.
doi:10.1371/journal.pone.0021531.g001

bioengineered teeth unit could be transplanted into an edentulous jaw (figure S2E, F). Our current findings suggest that bioengineered teeth can be engrafted into regions of tooth loss through bone integration, which involves resorption of the alveolar bone of the bioengineered tooth unit through natural bone remodeling in the recipient.

The engrafted bioengineered tooth was found to be aligned appropriately and occlude with the opposing upper first molar (figure 2E, figure S2C). Micro-CT analysis also revealed that no root elongation was evident for the bioengineered tooth and that the apical foramen of the engrafted bioengineered tooth root significantly narrowed at 40 days after transplantation (each n = 9; figure S2D). These results suggest that the bioengineered tooth in the tooth unit isolated from subrenal capsule transplantation is immature tooth, which has the potential to narrow of the apical foramen after the oral transplantation and would have the physiological ability to recapitulate mechanical stress by occlusion.

Masticatory potential is essential for proper tooth function and we next performed a Knoop hardness test, an important measure of masticatory functions, on bioengineered teeth including both the dentin and the enamel components. The Knoop hardness numbers (KHN) of the enamel and dentin in the natural teeth of 11-week-old adult mice were measured at 404.2±78.2 and 81.0±11.5, respectively (each n = 5, figure 2F). The bioengineered teeth generated in a subrenal capsule (SRC) and in jaw bone (TP) showed similar KHN values at 179.6±49.2 and 319.6±78.3 in the enamel, and 80.7±11.5 and 76.8±13.6 KHN in the dentin, respectively (each n = 5, figure 2F). The value of enamel Knoop hardness of natural tooth increase in according to postnatal period [20]. Although the enamel hardness of the bioengineered tooth generated in a SRC showed low KHN values, the enamel hardness of the engrafted bioengineered teeth (TP) increased to the high KHN value in according to the period after the transplantation into jaw bone. Therefore, the hardness of the dentin in the engrafted bioengineered teeth was in the normal range. These findings indicate that the hardness of the enamel and dentin in the engrafted bioengineered teeth were in the normal range.

Functional Analysis of the Periodontal Ligament and Neurons of the Engrafted Bioengineered Teeth

Previously, it had been demonstrated that the bioengineered tooth germ can recapitulate physiological tooth function in the adult murine oral environment [20]. In our present study, we next investigated whether an engrafted bioengineered mature tooth unit can also restore physiological tooth functions *in vivo* such as the response to mechanical stress and the perceptive potential for noxious stimulations. It is essential for tooth functions that the engrafted bioengineered tooth in recipient has the cooperation with the oral and maxillofacial regions through the PDL. The response of the PDL to mechanical stress, such as orthodontic movements, induces alveolar bone remodeling, which is indicated by the localization of tartrate-resistant acid phosphatase (TRAP)-osteoclasts and osteocalcin (*Ocn*) mRNA-positive osteoblasts [20]. During experimental tooth movement, TRAP-positive osteoclasts and *Ocn* mRNA-positive osteoblasts were observed on the compression and tension sides, respectively (figure 3A). This demonstrated that the PDL of the bioengineered tooth unit successfully mediates bone remodeling via the proper localization of osteoclasts and osteoblasts in response to mechanical stress.

The perceptive potential for noxious stimulation including mechanical stress and pain, are important for proper tooth function [30]. Trigeminal ganglional neurons, which innervate the pulp and PDL, can respond to these stimulations and transduce the perceptions to the central nervous system. Blood vessels that are detected in the pulp and PDL, maintain dental tissues such as odontoblasts, pulp, the PDL and alveolar bone. In our current experiments, we evaluated the responsiveness of nerve fibers in the pulp and PDL of the engrafted bioengineered tooth to noxious stimulations. Although von Willebrand Factor (vWF)-positive blood vessels were observed in the pulp and PDL of the bioengineered tooth generated in a subrenal capsule, anti-neurofilament (NF)-immunoreactive nerve fibers could not be detected (figure 3B, figure S3A, B). However, NF-positive nerve fibers could be detected in the pulp and PDL of the engrafted bioengineered tooth in the recipient bone and the neurons merged with vWF-positive blood vessels (figure 3B). Neuropeptide Y (NPY) and calcitonin gene-related peptide (CGRP), which are synthesized in sympathetic and sensory nerves, respectively, were also detected in both the pulp and PDL neurons (figure 3B, figure S3C–F). We found in our current analyses that c-Fos immunoreactive neurons, which are detectable in the superficial layers of the medullary dorsal horn following noxious stimulations such as mechanical and chemical stimulation of the intraoral receptive fields, were present in both normal and bioengineered teeth and drastically increased in number at two hours after orthodontic treatment and pulp exposure (figure 3C). These results indicate that an engrafted bioengineered tooth unit can indeed restore the

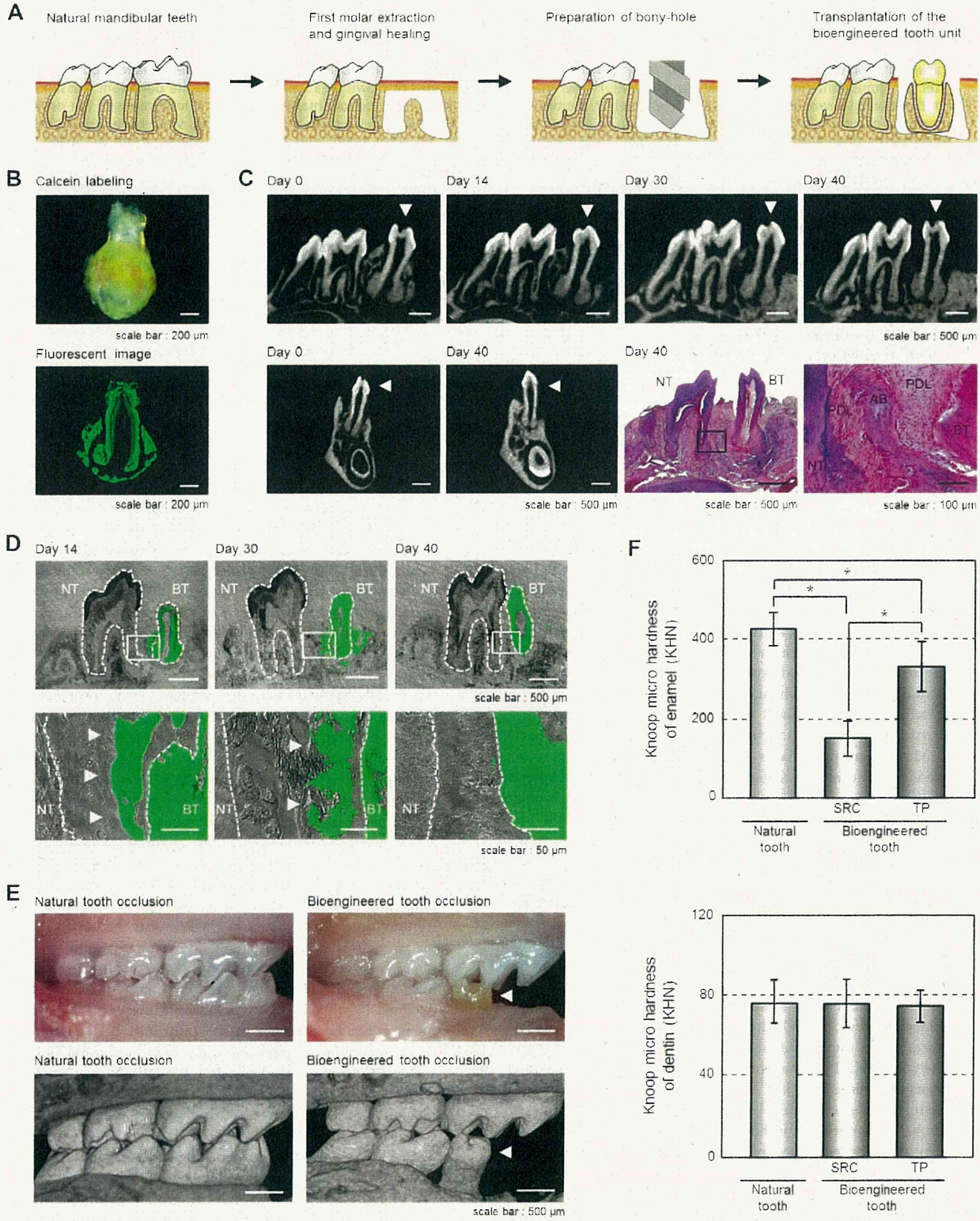

Figure 2. Engraftment and occlusion of a bioengineered tooth unit in a tooth loss model. (A) Schematic representation of the protocol used to transplant a bioengineered tooth unit in a murine tooth loss model. (B) Photograph (*Upper*) and sectional image (*Lower*) of a calcein-labeled bioengineered tooth unit at 60 days post transplantation in an SRC. Scale bar, 200 μm. (C) Micro-CT images of a bioengineered tooth unit (arrowhead) in cross section (*upper*) and frontal section (*first and second figures from the lower left*) during the processes of bone remodeling and

connection between the recipient jaw bone and alveolar bone of the tooth unit. Histological analysis of the engrafted bioengineered tooth unit at 40 days post transplantation was also performed. (Scale bar, 500 μm and 100 μm in the lower and higher magnification figure; *third and fourth figure from the lower left*). NT, natural tooth; BT, bioengineered tooth; AB, alveolar bone; PDL, periodontal ligament. (D) Sectional images of a calcein-labeled bioengineered tooth unit at 14, 30 and 40 days post-transplantation. The calcein-labeled bone of the bioengineered tooth units (arrowhead) was found to gradually decrease from the outside and finally disappear at 40 days post-transplantation. Scale bar, 500 μm (*upper*), 50 μm (*lower*). NT, natural tooth; BT, bioengineered tooth. (E) Oral photographs (*upper*) and micro-CT (*lower*) images showing occlusion of natural (*left*) and bioengineered teeth (*right*). Scale bar, 500 μm. (F) Assessment of the hardness of a bioengineered tooth. Knoop microhardness values of the enamel (*upper*) and dentin (*lower*) of a bioengineered tooth at 60 days post-transplantation in a subrenal capsule (SRC) and at 40 days post-transplantation in jawbone (TP) were compared with those of natural teeth in 11-week-old mice. Error bars show the standard deviation ($n = 5$). *$P<0.01$ (*t*-test).
doi:10.1371/journal.pone.0021531.g002

perceptive potential for noxious stimulations in cooperation with the maxillofacial region.

Regeneration of an Extensive Bone Defect by Transplantation of a Bioengineered Tooth Unit

Tooth loss is well known to cause significant alveolar bone resorption at the region in question [26]. Although there have been many studies of bone regenerative therapies [31], more effective methods to restore extensive bone defects during treatments such as dental implants are required and anticipated [26]. We investigated whether the transplantation of a bioengineered tooth unit would regenerate not only the missing tooth but also the surrounding alveolar bone of the recipient. To analyze whether such restoration of the alveolar bone occurred after transplantation, we developed a murine extensive bone defect model, which was prepared by the extraction of the lower first molar and then removal of the surrounding alveolar bone to generate a critical bone defect in the lower first molar region (figure 4A, figure S4A). When we transplanted a bioengineered tooth unit into this bone defect, vertical bone formation was observed from the marginal bone of the recipient at 14 days after transplantation (figure 4B, C, figure S4B). The regenerative bone volume post-transplantation significantly increased compared with a no transplant control (0.38 ± 0.07 mm^3 vs. 0.12 ± 0.08 mm^3; each $n = 4$, figure 4C, D), although the height and volume of the regenerated alveolar bone surrounding the bioengineered teeth was not completely recovered. These findings indicate that transplantation of a bioengineered tooth unit can restore a serious bone defect.

Discussion

We here demonstrate the successful transplantation of a bioengineered tooth unit, which is a model for a bioengineered mature organ, into a missing tooth region *in vivo* and the subsequent restoration of tooth function by this graft. We also show that this transplantation can restore the bone volume in both the vertical and horizontal dimensions in a missing tooth mouse model with a serious extensive bone defect. These findings indicate that whole tooth regenerative therapy is feasible through the transplantation of a bioengineered mature tooth unit. This study also provides the first reported evidence of entire organ regeneration through the transplantation of a bioengineered tooth.

Organ replacement regenerative therapy, but not stem cell transplantation regenerative therapy for tissue repair, holds great promise for the future replacement of a dysfunctional organ with a bioengineered organ reconstructed using three-dimensional cell manipulation *in vitro* [11,19]. In previous reports, however, artificial organs, which were constructed with various cells and artificial materials could not restore functionality and thus are not a viable option for long-term organ replacement *in vivo* [15]. Previously, it has been shown that a bioengineered organ can be grown *in vivo* in amphibian models in which activin-treated cell aggregates could form a secondary heart with pumping function and also regenerate eyes that were light responsive and connected with the host nervous system [32,33]. Recently, we have also regenerated bioengineered organ germs, including tooth germs and whisker follicles, and successfully achieved a fully functioning tooth replacement in an adult mouse through the transplantation of a bioengineered tooth germ in the lost tooth region [20,22]. It has been anticipated that replacement therapies will be developed in the future through the transplantation of a bioengineered mature organ with full functionality and long-term viability [2,19]. In our present experiments, we successfully generated a size-controlled bioengineered mature tooth unit, a strategy we adopted because the growth of functional organs *in vitro* is not yet possible [27]. Organs require a sufficient mass (cell number) and proper shape to function [34] and the tooth has unique morphological features, such as the tooth crown width and length (macro-morphology), and cusp and root shape (micro-morphology) [35]. However, the technology to regulate tooth morphogenesis for whole tooth regeneration remains unexplored [36]. We recently developed a novel organ germ method to regulate the crown width by regulating the contact area between epithelial and mesenchymal cell layers [28]. In our previous work, we demonstrated that the length of the bioengineered tooth is equivalent to that of natural tooth after the transplantation of the bioengineered tooth germ into oral environment [20]. In this study, the length of the bioengineered tooth unit could be controlled longitudinally, which would be provided by the limited space of the device. These findings provide the first evidence that the bioengineered tooth can be controlled in three-dimensions using a specialized device. It is also thought that bioengineered teeth could be generated with a controlled crown width through cell manipulation and tooth length by placement in a size-controlling device, which places a three-dimensional spatial limitation on size [20,28].

Loss of teeth and functional disorders in the PDL or temporomandibular joint, cause fundamental problems for oral functions, such as enunciation, mastication and occlusion, and associated health issues [21]. Although, missing teeth are traditionally restored by replacement with an artificial tooth, such as a bridge, denture or osseo-integrated dental implant, it is thought that the proper restoration of tooth functions will require bone remodeling regulated by the PDL [20] and a proper responsiveness to noxious stimulations [30]. Previous reports of autologous tooth transplantations have indicated that natural periodontal tissue on the tooth could restore the physiological tooth function, including bone remodeling [37]. We recently showed that a fully functional bioengineered tooth can be achieved through the transplantation of a bioengineered organ germ [20]. In our current study, we demonstrate the successful replacement of an entire and fully functional tooth unit *in vivo*, which restored masticatory potential, the functional responsiveness, including bone remodeling, of the periodontal tissue to mechanical stress and proper responsiveness to noxious stimulations via both peripheral sensory and sympathetic nerves. This is a significant

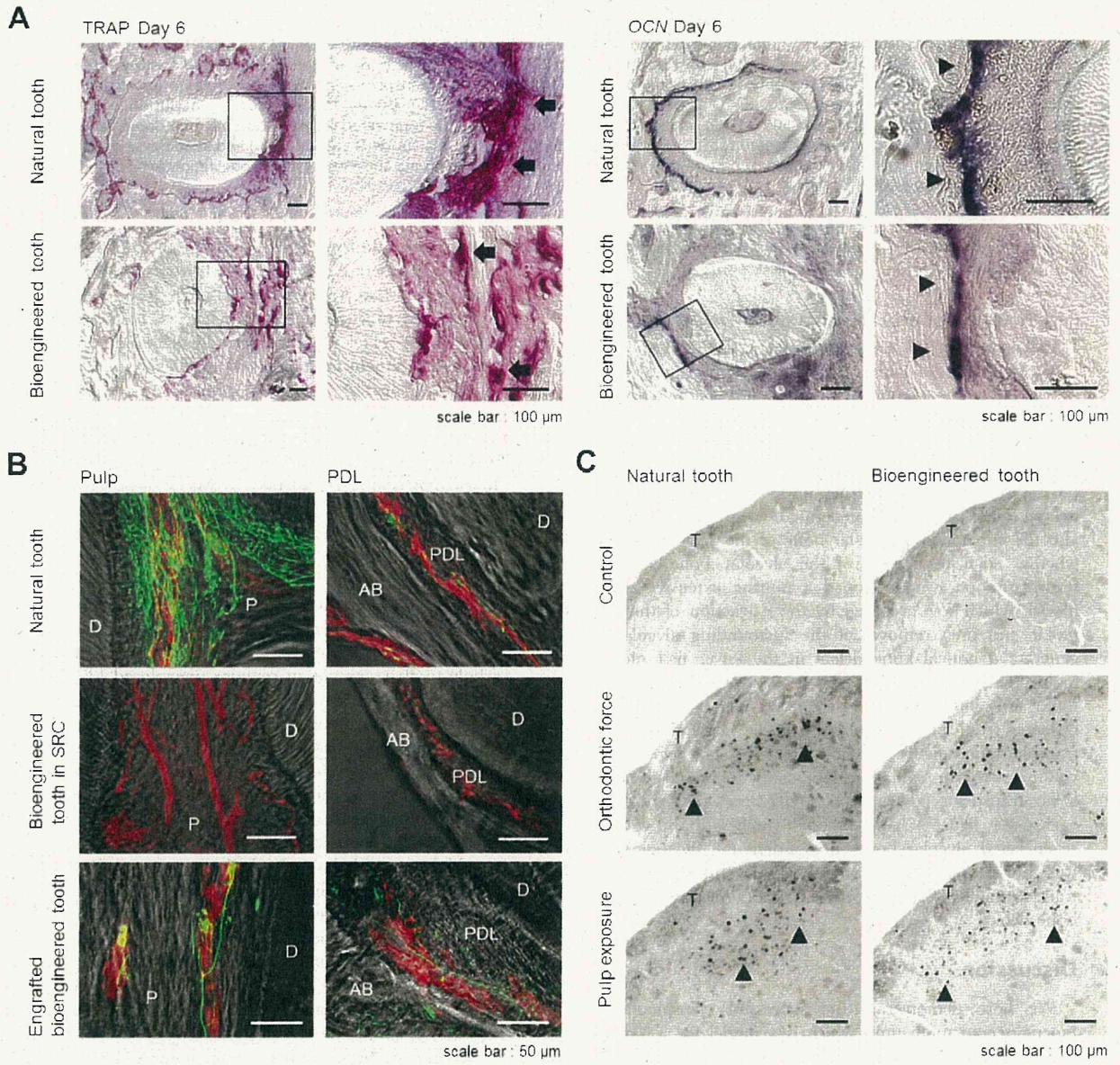

Figure 3. Experimental tooth movement and pain response to mechanical stress. (A) Sections of natural and bioengineered teeth were analyzed by TRAP-staining and *in situ* hybridization analysis of *Ocn* mRNA at day 6 of orthodontic treatment. TRAP-positive cells (arrow) and *Ocn* mRNA-positive cells (arrowhead) are indicated. Scale bar, 100 μm. (B) Nerve fibers and blood vessels in the pulp and PDL of a natural tooth (*top*), a bioengineered tooth unit in an SRC (*middle*), and a bioengineered tooth at 40 days after transplantation (*bottom*) were analyzed immunohistochemically using specific antibodies for neurofilament (NF; green) and von Willebrand Factor (vWF; red). Scale bar, 50 μm. D, dentin; P, pulp; AB, alveolar bone; PDL, periodontal ligament. (C) Analysis of c-Fos immunoreactive neurons in the medullary dorsal horns of mice after 0 hours (no stimulation, control; *top*), 2 hours of stimulation by orthodontic force (*middle*) and pulp exposure (*bottom*). C-Fos (arrowhead) was detectable after these stimulations in both natural (*left*) and bioengineered teeth at 40 days post-transplantation (*right*). Scale bar, 100 μm. T, spinal trigeminal tract.
doi:10.1371/journal.pone.0021531.g003

advance for the concept of whole tooth regenerative therapy in which the transplantation of a bioengineered mature organ, and not organ germ, can replace an organ and restore its full function.

In order for a tooth to cooperate with the maxillofacial region, it is supported by the connection between the root cementum and alveolar bone through the PDL, which has essential roles in tooth support, resorption and repair of the root cementum, and the remodeling of alveolar bone [38]. Tooth loss causes a large amount of alveolar bone resorption, which is mediated by the PDL, in the vertical and horizontal dimensions, and the loss of this bone, which leads to both functional and aesthetic problems, is difficult to rectify with standard dental therapies such as dental implant and autologous tooth transplantation [26]. Although bone regeneration has been attempted for many years through the use of tissue engineering technologies, guided bone regeneration methods, autologous bone or cell transplantation, and cytokine

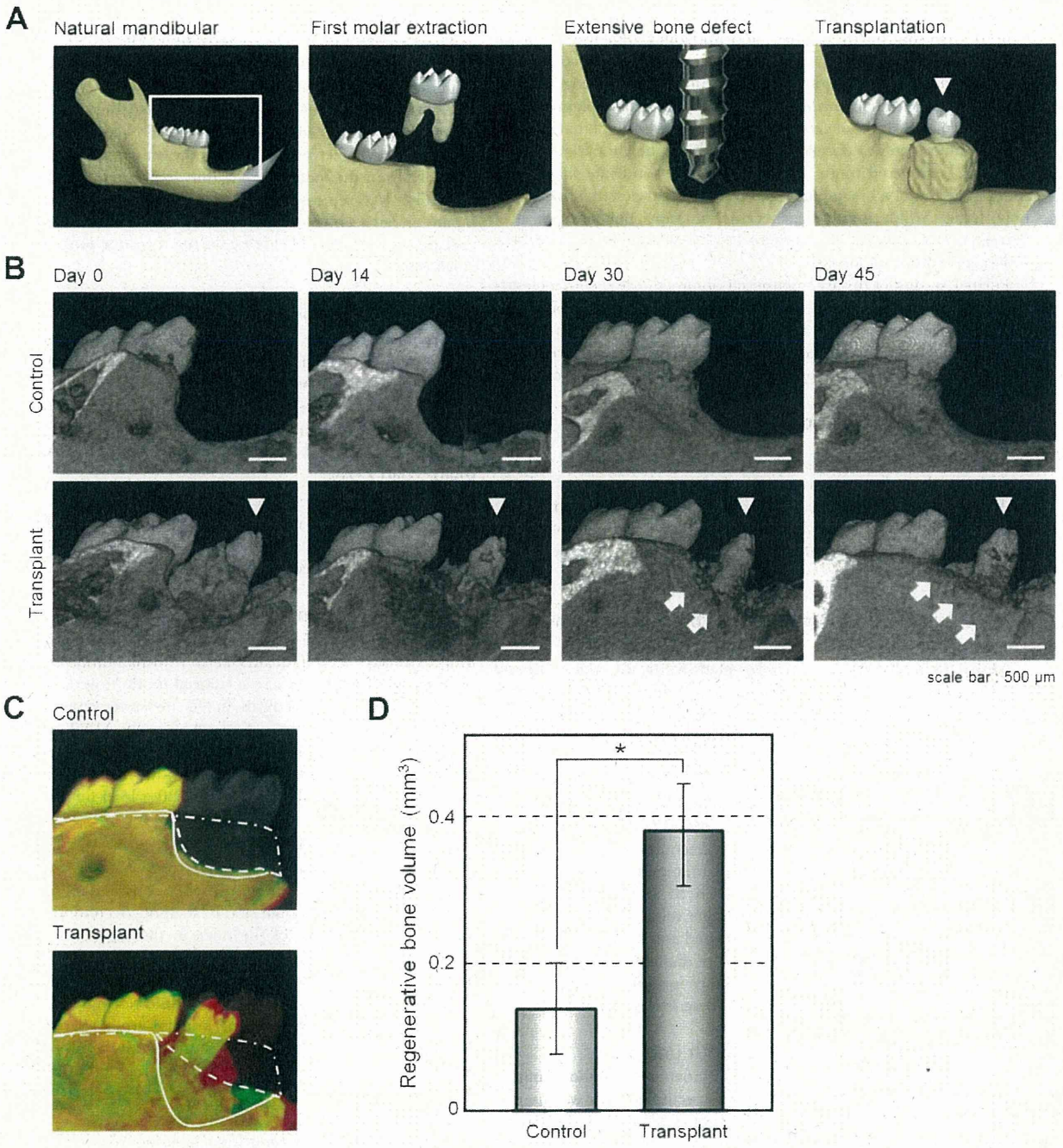

Figure 4. Alveolar bone regeneration following the transplantation of a bioengineered tooth unit. (A) Schematic representation of a murine extensive bone defect model and the transplantation of a bioengineered tooth unit (arrowhead). (B) Micro-CT images of the vertical alveolar bone regeneration processes in a no transplantation control (*upper*) and following the transplantation of a bioengineered tooth unit (arrowhead, *lower*) in a murine extensive bone defect model. Vertical bone formation was observed from the marginal bone of the recipient (arrow). Scale bar, 500 μm. (C) Three-dimensional superposition of micro-CT images of natural dentition (gray, double dotted line), a transplanted bioengineered tooth unit (*lower*) and a no transplantation control (*upper*) at day 0 in an extensive bone defect (red, straight line), and at 45 days after transplantation (green, dotted line). The superior edges of the recipient alveolar bone are indicated by each line. (D) Regenerative bone volume of the buccal area following the transplantation of a bioengineered tooth unit (transplant) and no transplantation (control) at day 45 in an extensive bone defect. Error bars show the standard deviation ($n = 4$). *$P < 0.01$ (*t*-test).
doi:10.1371/journal.pone.0021531.g004

therapies with BMPs, FGFs or PDGF, no clinical protocol for bone regeneration in the vertical and horizontal dimensions has been established yet [31]. In our present study however, we demonstrate that a bioengineered tooth unit could be engrafted and integrate via recipient bone remodeling after transplantation into an extensive bone defect. The recipient alveolar bone of the vertical dimension was observed to maintain the height of the PDL in the bioengineered tooth unit. These findings indicate that the transplantation of a bioengineered tooth has great potential for not only future whole tooth regenerative therapy but also as a treatment in clinical cases where tooth loss is accompanied by a serious alveolar bone defect.

Further studies of three-dimensional organ culture technologies *in vitro*, which can generate a fully functional bioengineered organ, and the identification of available adult tissue stem cells for the reconstitution of a bioengineered tooth germ will be required in the future to realize whole tooth regenerative therapy in the clinic.

Materials and Methods

Ethics Statement

All animals and experimental protocols were approved by the Tokyo University of Science Animal Care and Use Committee (Permit Number: N10018). All surgery was performed under sodium pentobarbital anesthesia, and all efforts were made to minimize suffering.

Reconstitution of a bioengineered tooth germ from single cells

Molar tooth germs were dissected from the mandibles of ED14.5 mice. The isolation of tissues and single cell preparations from the epithelium and mesenchyme has been described previously [22]. Dissociated epithelial and mesenchymal cells were precipitated by centrifugation in a siliconized microtube and the supernatant was completely removed. The cell density of the precipitated epithelial and mesenchymal cells after the removal of the supernatants reached a concentration of 5×10^8 cells/ml [22]. Bioengineered molar tooth germ was reconstituted using our previously described 3-dimensional cell manipulation technique, the organ germ method [22]. We used 5×10^4 epithelial and mesenchymal cells each to generate single tooth structures. The bioengineered tooth germs were incubated for 10 min at 37°C, placed on a cell culture insert (0.4 μm pore diameter; BD, Franklin Lakes, New Jersey, USA), and then further incubated at 37°C for five days in an *in vitro* organ culture as described previously [22].

Generation of a bioengineered tooth unit

To control the length and shape of the bioengineered tooth unit, we manufactured a plastic ring-shaped structure, which was used as a size-control device, of a 1.3, 1.8 or 2.5 mm inside diameter and 1.3 mm thickness. After five days of cultivation, the reconstituted tooth germs were placed into this spacing device which was transplanted into a subrenal capsule for 60 days using 7-week-old female mice as the hosts. The bioengineered tooth unit was then isolated from the device.

Fluorescent calcein labeling

Calcein (Wako, Osaka, Japan) was administered daily (1.6 mg/kg) via a subcutaneous dose to the transplanted bioengineered tooth germ in the subrenal capsule. These tooth units were then transplanted into the extracted regions of a lower first molar for 14, 30 or 40 days. Non-decalcified frozen sections were then prepared and observed using an Axiovert (Carl Zeiss, Oberkochen, Germany) with AxioCAM MRc5 (Carl Zeiss).

Transplantation

The lower first molars of 4-week-old C57BL/6 (SLC, Shizuoka, Japan) mice were extracted under deep anesthesia and the resulting gingival wounds had been allowed to heal for 4–6 days. The transplantation of a bioengineered tooth unit was allowed the procedure as described previously [20]. To generate an extensive alveolar bone defect mouse model, the whole supporting alveolar bone (1.5 mm mesiodistally, 1.2 mm buccolingually and 0.6 mm vertically) was removed using a dental engine (NSK, Tochigi, Japan) under deep anesthesia. The bioengineered tooth units were transplanted into these defects using the same procedure described above.

Microcomputed Tomography (Micro-CT)

The heads of the mice that had received a transplanted bioengineered tooth unit and normal mice were arranged in the centric occlusal position and radiographic imaging was then performed by x-ray using a Micro-CT device (R_mCT; Rigaku, Tokyo, Japan) with exposure at 90 kV and 150 mA. Micro-CT images were captured using i-view R (Morita, Kyoto, Japan) and Imaris (Carl Zeiss).

Histochemical analysis and immunohistochemistry

Histochemical and immunohistochemical tissue analyses were performed as described previously [20,22].

Hardness measurements

Polished enamel and dentin samples from bioengineered tooth units extracted at 60 days after germ transplantation into the SRC or the mandible, and also a normal tooth (9-week postnatal) were embedded in acrylic resin ($n = 5$ for each group). The Knoop hardness test was then performed using a Miniload Hardness Tester (HM-102; Mitutoyo, Kanagawa, Japan) equipped with a Knoop diamond tip (19BAA061; Mitutoyo). Five indentations were made on each specimen with a 10 g load for 10 sec.

Experimental orthodontic treatments

Orthodontic treatment was performed as described previously [20]. Experimental tooth movements consisted of a horizontal orthodontic force of about 10–15 g applied continuously to the bioengineered tooth of the mice in the experimental group in a buccal direction using a dial tension gauge (Mitutoyo) for six days. In the control group, orthodontic force was applied in the buccal direction to the first molars of 7-week-old normal C57BL/6 mice in the same manner as the experimental group. Serial sections at day 6 were analyzed by TRAP staining and by *in situ* hybridization analysis for osteocalcin (*Ocn*) mRNA as previously described [20].

Pulp exposure

A minimal pinpoint mechanical exposure of the pulp was made in the bioengineered tooth or control natural first molar of mice under anesthesia using a dental engine (NSK) supplied with dental diamond point (Shofu, Kyoto, Japan). For stimulation with cold water, ice was applied to the cavity of the tooth after pulp exposure.

Measurement of the regenerative bone volume

To evaluate the extent of the alveolar bone recovery in our extensive bone defect mouse model, we used the Micro-CT device (Rigaku) to measure alveolar bone volume of the treated areas at 0 and 45 days after transplantation. We measured the volume of the alveolar bone in the operated region using TRI/3D-BON software (Ratoc, Osaka, Japan). The 3D region of interest (ROI)

was selected in the buccal alveolar bone area which was prescribed from the medial edge of lower second molar to the distal edge of the foramen mentale. We subtracted the alveolar bone volume of the area at day 0 from the volume at day 45, and calculated the regenerated bone volume.

Statistical analysis

Statistical significance was determined with the unpaired Student's *t*-test, analyzed using the Common Gateway Interface Program (twk, Saint John's University).

Supporting Information

Figure S1 A method for controlling the size of a bioengineered tooth unit. (A) Micro-CT images of the shapes of a bioengineered tooth unit, size controlled by devices of a 1.3 or 1.8 mm inner diameter, at 30 and 60 days after transplantation in an SRC. Scale bar, 500 μm. (B) Photograph of plural bioengineered tooth germ arranged in a size controlled device. Scale bar, 500 μm. (C) Micro-CT images (*left*) and histological analysis of the multiple bioengineered tooth units on day 60 after SRC transplantation (*middle and right*). The alveolar bone between the bioengineered teeth is indicated by arrowheads (*lower left*). Scale bar, 200 μm. Higher magnification images of the periodontal tissue area (*lower middle and right*) are also shown. Scale bar, 50 μm. D, dentin; AB, alveolar bone; PDL, periodontal ligament.
(TIF)

Figure S2 Engraftment and establishment of occlusion of a bioengineered tooth unit at the tooth loss region. (A) Oral photographs and micro-CT images of bioengineered tooth unit transplantations into the adult mandible. Images were captured of lateral (*top*), occlusal (*middle*) and cross sections (*bottom*) views. The bioengineered tooth unit is indicated by an arrowhead. Scale bar, 500 μm. (B) Sectional images of a calcein-labeled bioengineered tooth unit at 14, 30 and 40 days after transplantation into a murine model. Fluorescent and DIC images are merged. The alveolar bone of the bioengineered tooth unit is indicated by arrowheads. Scale bar, 500 μm, *upper*; 100 μm, *lower*. NT, natural tooth; BT, bioengineered tooth. (C) Oral photographs of an engrafted bioengineered tooth in a lateral view (upper left), a 45-degree view (*lower left*), an occlusal view (*upper right*) and a fluorescent image (*lower right*). Scale bar, 500 μm. (D) Measurements of the tooth length (*left*) and apical foramen width (*right*) of a bioengineered tooth at day 0 and day 40 after transplantation. Error bars show the standard deviation ($n = 9$). $^*P<0.05$ (*t*-test). (E) Schematic representation of the protocol for transplanting multiple bioengineered tooth units in a murine edentulous model. (F) Micro-CT images of transplanted multiple bioengineered tooth units in a murine edentulous model. Images were captured of the external surface area (*left*), sagittal section (*center*) and cross section (*right*). The bioengineered teeth are indicated by the arrowheads in *the left figure*. Scale bar, 500 μm.
(TIF)

Figure S3 Regeneration of nerve fibers and blood vessels in the engrafted bioengineered tooth unit. (A, B) Nerve fibers and blood vessels in the pulp (A) and PDL (B) of a natural tooth (*top*), bioengineered tooth unit in an SRC (*middle*) and bioengineered tooth at 40 days after transplantation into an oral tooth loss region (*bottom*) were analyzed immunohistochemically using specific antibodies for NF and vWF. DIC (*first columns from the left*), NF images (*second columns*), vWF images (*third columns*), and merged images (*fourth columns*) are shown. Scale bar, 50 μm. (C, D) Nerve fibers in the pulp (C) and PDL (D) of a natural tooth (*top*), bioengineered tooth unit in an SRC (*middle*) and bioengineered tooth at 40 days after transplantation (*bottom*) were analyzed immunohistochemically using specific antibodies for NF and neuropeptide Y (NPY). DIC (*first columns from the left*), NF images (*second columns*), NPY images (*third columns*), and merged images (*fourth columns*) are shown. Scale bar, 50 μm. (E, F) Nerve fibers in the pulp (E) and PDL (F) of a natural tooth (*top*), bioengineered tooth unit in an SRC (*middle*) and bioengineered tooth at 40 days after transplantation (*bottom*) were analyzed immunohistochemically using specific antibodies for NF and calcitonin gene-related peptide (CGRP). DIC (*first columns from the left*), NF images (*second columns*), CGRP images (*third columns*), and merged images (*fourth columns*) are shown. Scale bar, 50 μm.
(TIF)

Figure S4 Alveolar bone regenerative potential of a bioengineered tooth unit. (A) Photographs of a lateral (*left*) and occlusal (*right*) view of a natural mandibular dentition and an extensive bone defect (arrowhead). Scale bar, 500 μm. (B) Micro-CT images of the frontal section of a no transplantation control (*upper*) and a transplanted bioengineered tooth unit at day 45 in a murine extensive bone defect model (*lower*). Significant vertical bone regeneration was observed following the transplantation of a bioengineered tooth unit when compared with the no transplantation control. The regenerated alveolar bone is indicated by an arrow. Scale bar, 500 μm.
(TIF)

Author Contributions

Performed the experiments: M. Oshima MM MY KN. Analyzed the data: AI M. Ogawa HY. Wrote the paper: M. Oshima TT. Designed the research plan: TT M. Oshima. Developed new assay systems and the discussion of the results: M. Ogawa RM EI TT-Y SK MS.

References

1. Lechler RI, Sykes M, Thomson AW, Turka LA (2005) Organ transplantation how much of the promise has been realized? Nat Med 11: 605–613.
2. Gridelli B, Remuzzi G (2000) Strategies for making more organs available for transplantation. N Engl J Med 343: 404–410.
3. Moers C, Smits JM, Maathuis MH, Treckmann J, van Gelder F, et al. (2009) Machine perfusion or cold storage in deceased-donor kidney transplantation. N Engl J Med 360: 7–19.
4. Copelan EA (2006) Hematopoietic stem-cell transplantation. N Engl J Med 354: 1813–1826.
5. Nishikawa S, Goldstein RA, Nierras CR (2008) The promise of human induced pluripotent stem cells for research and therapy. Nat Rev Mol Cell Biol 9: 725–729.
6. Miyahara Y, Nagaya N, Kataoka M, Yanagawa B, Tanaka K, et al. (2006) Monolayered mesenchymal stem cells repair scarred myocardium after myocardial infarction. Nat Med 12: 459–465.
7. Ohashi K, Yokoyama T, Yamato M, Kuge H, Kanehiro H, et al. (2007) Engineering functional two- and three-dimensional liver systems in vivo using hepatic tissue sheets. Nat Med 13: 880–885.
8. Korbling M, Estrov Z (2003) Adult stem cells for tissue repair - a new therapeutic concept? N Engl J Med 349: 570–582.
9. Atala A (2005) Tissue engineering, stem cells and cloning: current concepts and changing trends. Expert Opin Biol Ther 5: 879–892.
10. Purnell B (2008) New release: the complete guide to organ repair. Introduction Science 322: 1489.
11. Ikeda E, Tsuji T (2008) Growing bioengineered teeth from single cells: potential for dental regenerative medicine. Expert Opin Biol Ther 8: 735–744.
12. Layer PG, Robitzki A, Rothermel A, Willbold E (2002) Of layers and spheres: the reaggregate approach in tissue engineering. Trends Neurosci 25: 131–134.
13. Yelick PC, Vacanti JP (2006) Bioengineered teeth from tooth bud cells. Dent Clin North Am 50: 191–203, viii.
14. Khademhosseini A, Langer R, Borenstein J, Vacanti JP (2006) Microscale technologies for tissue engineering and biology. Proc Natl Acad Sci U S A 103: 2480–2487.
15. Uygun BE, Soto-Gutierrez A, Yagi H, Izamis ML, Guzzardi MA, et al. (2010) Organ reengineering through development of a transplantable recellularized liver graft using decellularized liver matrix. Nat Med 16: 814–820.

16. Zheng Y, Du X, Wang W, Boucher M, Parimoo S, et al. (2005) Organogenesis from dissociated cells: generation of mature cycling hair follicles from skin-derived cells. J Invest Dermatol 124: 867–876.
17. Shackleton M, Vaillant F, Simpson KJ, Stingl J, Smyth GK, et al. (2006) Generation of a functional mammary gland from a single stem cell. Nature 439: 84–88.
18. Yen AH, Sharpe PT (2006) Regeneration of teeth using stem cell-based tissue engineering. Expert Opin Biol Ther 6: 9–16.
19. Sharpe PT, Young CS (2005) Test-tube teeth. Sci Am 293: 34–41.
20. Ikeda E, Morita R, Nakao K, Ishida K, Nakamura T, et al. (2009) Fully functional bioengineered tooth replacement as an organ replacement therapy. Proc Natl Acad Sci U S A 106: 13475–13480.
21. Nickel JC, Iwasaki LR, Walker RD, McLachlan KR, McCall WD, Jr. (2003) Human masticatory muscle forces during static biting. J Dent Res 82: 212–217.
22. Nakao K, Morita R, Saji Y, Ishida K, Tomita Y, et al. (2007) The development of a bioengineered organ germ method. Nat Methods 4: 227–230.
23. Zaret KS, Grompe M (2008) Generation and regeneration of cells of the liver and pancreas. Science 322: 1490–1494.
24. Slack JM (2008) Origin of stem cells in organogenesis. Science 322: 1498–1501.
25. Hu B, Nadiri A, Kuchler-Bopp S, Perrin-Schmitt F, Peters H, et al. (2006) Tissue engineering of tooth crown, root, and periodontium. Tissue Eng 12: 2069–2075.
26. Van der Weijden F, Dell'Acqua F, Slot DE (2009) Alveolar bone dimensional changes of post-extraction sockets in humans: a systematic review. J Clin Periodontol 36: 1048–1058.
27. Wang X, Yan Y, Zhang R (2010) Recent trends and challenges in complex organ manufacturing. Tissue Eng Part B Rev 16: 189–197.
28. Ishida K, Murofushi M, Nakao K, Morita R, Ogawa M, et al. (2011) The regulation of tooth morphogenesis is associated with epithelial cell proliferation and the expression of Sonic hedgehog through epithelial-mesenchymal interactions. Biochem Biophys Res Commun 405: 455–461.
29. Geertman ME, Slagter AP, van Waas MA, Kalk W (1994) Comminution of food with mandibular implant-retained overdentures. J Dent Res 73: 1858–1864.
30. Byers MR, Narhi MV (1999) Dental injury models: experimental tools for understanding neuroinflammatory interactions and polymodal nociceptor functions. Crit Rev Oral Biol Med 10: 4–39.
31. Bueno EM, Glowacki J (2009) Cell-free and cell-based approaches for bone regeneration. Nat Rev Rheumatol 5: 685–697.
32. Kinoshita M, Ariizumi T, Yuasa S, Miyoshi S, Komazaki S, et al. (2010) Creating frog heart as an organ: in vitro-induced heart functions as a circulatory organ in vivo. Int J Dev Biol 54: 851–856.
33. Sedohara A, Komazaki S, Asashima M (2003) In vitro induction and transplantation of eye during early Xenopus development. Dev Growth Differ 45: 463–471.
34. Tyler D, Baker NE (2003) Size isn't everything. Bioessays 25: 5–8.
35. Cai J, Cho SW, Kim JY, Lee MJ, Cha YG, et al. (2007) Patterning the size and number of tooth and its cusps. Dev Biol 304: 499–507.
36. Jernvall J, Thesleff I (2000) Reiterative signaling and patterning during mammalian tooth morphogenesis. Mech Dev 92: 19–29.
37. Kallu R, Vinckier F, Politis C, Mwalili S, Willems G (2005) Tooth transplantations: a descriptive retrospective study. Int J Oral Maxillofac Surg 34: 745–755.
38. Cho MI, Garant PR (2000) Development and general structure of the periodontium. Periodontol 2000 24: 9–27.

JOURNAL OF DENTISTRY 39 (2011) 599–603

available at www.sciencedirect.com

ScienceDirect

journal homepage: www.intl.elsevierhealth.com/journals/jden

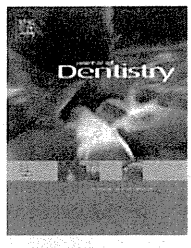

Cytotoxicity of 45S5 bioglass paste used for dentine hypersensitivity treatment

Ahmed Samir Bakry [a,b,c,*], *Yukihiko Tamura* [d], *Masayuki Otsuki* [a], *Shohei Kasugai* [e], *Keiichi Ohya* [d], *Junji Tagami* [a,f]

[a] *Cariology and Operative Dentistry Department, Graduate school of Medical and Dental Sciences, Tokyo Medical and Dental University, Tokyo, Japan*

[b] *Conservative Dentistry Department, Faculty of Dentistry, Alexandria University, Egypt*

[c] *Faculty of Dentistry, King Abdulaziz University, Saudia Arabia*

[d] *Pharmacology, Department of Hard Tissue Engineering, Graduate school of Medical and Dental Sciences, Tokyo Medical and Dental University, Tokyo, Japan*

[e] *Oral Implantology and Regenerative Dental Medicine Graduate School, Tokyo Medical and Dental University, Tokyo, Japan*

[f] *Global Center of Excellence Program, ICTB at Tokyo Medical and Dental University, Tokyo, Japan*

ARTICLE INFO

Article history:
Received 8 December 2010
Received in revised form
13 June 2011
Accepted 16 June 2011

Keywords:
45S5 bioglass
Bioactive glass
Cytotoxicity
Pulp cells
Dentine hypersensitivity

ABSTRACT

Objectives: 45S5 bioglass mixed with 50% phosphoric acid has been suggested to treat dentine hypersensitivity and incipient enamel caries. This study is going to evaluate the biocompatibility of using the aforementioned technique with the rat pulpal cells.

Methods: The relative cytotoxicity of 45S5 bioglass on rat dental pulp cells was compared to the cytotoxicity of a temporary filling material (Caviton; GC, Japan), Type 1 glass ionomer cement (Fuji I; GC, Tokyo, Japan) and commercial desensitising agent (SuperSeal; Phoenix Dental, Fenton, MI, USA) using a transwell insert model. Cell viability was measured by means of a 3-(4,5-dimethylthiazol-2-yl)-2,5-diphenyltetrazolium bromide (MTT) assay. The number of viable cell counts were compared using one way ANOVA ($p < 0.05$). The morphological alterations of the pulp cells were observed directly by phase contrast microscope.

Results: The results of this study indicated that cell viability recorded by the 45S5 bioglass paste group did not differ significantly from those of the Caviton, glass ionomer or superseal, moreover pulpal cells microscopic analysis revealed that 45S5 bioglass elicited minimal toxic effect.

Conclusions: 45S5 bioglass paste can serve as a biocompatible material that can potentially be used safely on dentine.

1. Introduction

Dentine hypersensitivity is one of the major challenges in dental practice.[1] The prevalence of dentine hypersensitivity varies from 4% to 57%[2] whilst the prevalence of dentine hypersensitivity is between 60% and 98% in patients with suffering from periodontitis.[3] The hydrodynamic theory[4,5] explains the phenomenon of dentine hypersensitivity as an increase in the flow of the fluids present in dentinal-tubules that have patent orifices, thereby activating nerves situated in the outer layers of the pulp. Exposure of dentinal-tubules orifices may be caused by many factors, such as acid erosion,[6–10] attrition, abrasion,[11] parafunctional habits or gingival

* *Corresponding author at*: Tokyo Medical and Dental University, Japan. Tel.: +81 3 5803 5483; fax: +81 3 5803 0195.
E-mail addresses: drahmedbakry@gmail.com, bakry.ope@tmd.ac.jp (A.S. Bakry).

0300-5712/$ – see front matter
doi:10.1016/j.jdent.2011.06.003

recession.[12] These dentinal-tubule orifices require permanent blocking as a treatment approach.[1,13–15]

Agents employed for treating dentine hypersensitivity show only temporary effect clinically because they are gradually removed by daily brushing, food friction, and change in the pH in the oral cavity.[10]

Bioactive glasses such as 45S5 bioglass can interact with the hard tissues by forming a calcium phosphate-rich layer which can bond chemically to these hard tissues.[16–18] We have previously reported that a 45S5 bioglass–50% phosphoric acid paste can form a crystallised calcium phosphate rich layer that can penetrate within the dentinal tubules' orifices; this layer was reported to be durable to brushing-abrasion wear challenge which suggests the possibility of using this technique for treating dentine hypersensitivity effectively.[19,20] However, there is no report about the biocompatibility of this technique.

The objective of this study was to compare the cytotoxicity of 45S5 bioglass on rat colonal dental pulp cells to the cytotoxicity of a temporary filling material containing zinc oxide (Caviton; GC, Japan), Type 1 glass ionomer cement (Fuji I; GC, Tokyo, Japan) and an oxalic acid containing desensitising agent (SuperSeal; Phoenix Dental, Fenton, MI, USA) using a transwell insert model by means of a 3-(4,5-dimethylthiazol-2-yl)-2,5-diphenyltetrazolium bromide (MTT) assay.

The hypothesis in this study was that 45S5 bioglass paste will show an acceptable biocompatibility when compared to the other tested materials.

2. Materials and methods

2.1. *Culture of (RPC-C2A) dental pulp cells*

The colonal cell line (RPC-C2A) established from dental pulp of rat incisor[21] were used in this study. The culture medium was Dulbecco's modified Eagle's medium (DMEM), supplemented with 10% foetal bovine serum (FBS) and antibiotic solution (60 μg/ml of kanamycin), under a humidified atmosphere of 95% air, 5% CO_2 and maintained at 37 °C.

2.2. *Cytotoxicity evaluation with the transwell insert model*

The tested materials included a temporary filling material (Caviton; GC, Japan), Type 1 glass ionomer cement (Fuji I; GC, Tokyo, Japan) and a commercially available desensitising agent (SuperSeal; Phoenix Dental, Fenton, MI, USA), and 45S5 bioglass (NovaMin®, 5 μm average particle, NovaMin Technology, Florida, USA), whilst a number of empty inserts served as the control group. All materials were sterilized by gas sterilization before cytotoxicity testing. The transwells used in this study were 6.5 mm in diameter, with a pore size of 0.4 μm (Costar Transwell-Clear, Corning Costa, Cambridge, MA). The transwells were transferred into 24-well culture plates that were seeded with pulp cells (5×10^3 cells/well) and kept for 24 h.

2.3. *Application of the tested materials in the transwells*

For the 45S5 bioglass, one tenth of a gram of 45S5 bioglass powder composed of (Na_2O, CaO, P_2O_5, SiO_2) was mixed on a glass slab for 1 min by spatula with 0.2 ml of 50% phosphoric acid that was prepared by diluting 85% phosphoric acid (Wako Chemicals, Osaka, Japan) in distilled water to form a gel (pH 2.2). The three other dental materials were manipulated according to their manufacturers' instructions and were applied as well as the 45S5 bioglass paste on the base of the transwells to form a 2 mm height of each material.[22]

Pulp cells in all groups exposed to the respective dental material and controls were then incubated for 3 days under a humidified CO_2 incubator at 37 °C. All of the transwells were then removed from the incubator, and the cell viability was measured using an MTT assay. For the MTT assay, the cells in each well were incubated with a culture medium containing 100 μL MTT (Roche) solutions for a period of 3 h at 37 °C. Only viable cells that feature functional mitochondria are able to reduce MTT to insoluble purple formazan crystals. Subsequently to this incubation, the medium was aspirated and 200 ml dimethyl sulfoxide (DMSO) was added to dissolve the reduced formazan crystals. The resultant solution was then lightly shaken for 15 min by a microplate shaker. The optical density (OD_{570}) of the formazan solution, which is directly proportional to the number of viable cells present in the solution, was measured with a microplate reader (Model 450, Bio-Rad [Bio-Rad Laboratories, CA]). A blank well was regularly used for data subtraction by placing the same volume of culture medium with MTT into culture wells that contained a transwell but no dental materials. Results of the MTT assay were analysed using one-way analysis of variance (ANOVA) followed by a Tukey test ($p < 0.05$) in order to determine whether any significant difference existed between the tested dental materials as regards relative toxicity to cultured dental-pulp cells.

2.4. *Morphological observation of the cultured pulp cells*

Morphological observations of the pulp cells were conducted using phase contrast microscope and then photographed using an Olympus camera.

Table 1 – Materials used in this study.

Materials	Composition	Procedures
45S5 bioglass (NovaMin® Technology, USA)	SiO_2 (45 wt%), Na_2O (24.5 wt%), CaO (24.4 wt%) and P_2O_5 (6 wt%)	Mix 0.1 g of 45S5 bioglass to 0.2 ml of 50% phosphoric acid
Caviton (GC Corporation, Tokyo, Japan)	Zinc oxide, plaster of Paris, vinyl acetate, ethanol	Apply directly
Fuji I (GC Corporation, Tokyo, Japan)	Powder: alumino-silicate glass Liquid: polyacrylic acid, water	Apply one scoop of powder to one drop of liquid
SuperSeal (Phoenix Dental, Fenton, MI, USA)	Oxalic acid, potassium salt	Apply directly